PHYSICAL REVIEW D **92,** 114022 (2015)

Exclusive decays $B \to \ell^- \bar{\nu}$ and $B \to D^{(*)} \ell^- \bar{\nu}$ in the covariant quark model

M. A. Ivanov,[1,*] Jürgen G. Körner,[2,†] and C. T. Tran[1,3,4,‡]

[1]*Bogoliubov Laboratory of Theoretical Physics, Joint Institute for Nuclear Research, 141980 Dubna, Russia*

[2]*PRISMA Cluster of Excellence, Institut für Physik, Johannes Gutenberg-Universität, D-55099 Mainz, Germany*

[3]*Advanced Center for Physics, Institute of Physics, Vietnam Academy of Science and Technology, 100000 Hanoi, Vietnam*

[4]*Department of General and Applied Physics, Moscow Institute of Physics and Technology, 141700 Dolgoprudny, Russia*

(Received 11 August 2015; published 22 December 2015)

We study the exclusive leptonic and semileptonic B decays $B \to \ell^- \bar{\nu}_\ell$ and $B \to D^{(*)} \ell^- \bar{\nu}_\ell$ in the framework of the covariant quark model with built-in infrared confinement. We compute the relevant form factors in the full kinematical momentum transfer region. The calculated form factors are used to evaluate branching fractions and polarization observables of the above transitions. We compare our results with experimental data and results from other theoretical studies.

DOI: 10.1103/PhysRevD.92.114022 PACS numbers: 12.39.Ki, 13.30.Eg, 14.20.Jn, 14.20.Mr

I. INTRODUCTION

The decays $B \to \ell^- \bar{\nu}$ and $B \to D^{(*)} \ell^- \bar{\nu} (\ell = e, \mu, \tau)$ play a prominent role in testing the Standard Model (SM) and looking for hints of New Physics (NP) in charged-current interactions. In the SM scenario a measurement of these decays provides a direct route to determining values of the B-meson decay constant f_B and the semileptonic form factors. They also help to determine the Cabibbo-Kobayashi-Maskawa (CKM) matrix elements $|V_{ub}|$ and $|V_{cb}|$ to a better precision. A puzzling feature of these decays is that there have been some recent hints that lepton universality is broken in the tauonic modes of these decays.

The leptonic and semileptonic modes are difficult to measure experimentally due to the presence of a neutrino in the final state. Ideal in this regard are B factories where a B-meson pair is generated from the process $e^+e^- \to \Upsilon(4S) \to B\bar{B}$. One of the B mesons ($B_{\rm tag}$) is then reconstructed in hadronic or semileptonic modes, while signal decays of the other B meson ($B_{\rm sig}$) are identified. A new player has entered the game in that the LHCb Collaboration has been able to identify the semileptonic decays $\bar{B}^0 \to D^* \tau^- \bar{\nu}_\tau$ and $\bar{B}^0 \to D^* \mu^- \bar{\nu}_\mu$ in hadronic collisions [1].

Since the first evidence reported by the Belle Collaboration in 2006 [2], many measurements of the branching fraction $\mathcal{B}(B^- \to \tau^- \bar{\nu}_\tau)$ have been reported by both the Belle and *BABAR* collaborations. There had been a consistent excess compared to the SM prediction until Belle published their result of $\mathcal{B}(B^- \to \tau^- \bar{\nu}_\tau) = [(7.2^{+2.7}_{-2.5}(\text{stat}) \pm 1.1(\text{syst}))] \times 10^{-5}$ with a significance of 3.0σ [3]. This result reduced the tension between theory and experiment and decreased the world average of the measured branching fraction to the recent value of $\mathcal{B}(B^- \to \tau^- \bar{\nu}_\tau) = (11.4 \pm 2.2) \times 10^{-5}$ [4], which is slightly larger than the SM expectation $(8.1 \pm 0.7) \times 10^{-5}$ obtained from a global fit to CKM matrix elements [4]. Note that the most recent result of $\mathcal{B}(B^- \to \tau^- \bar{\nu}_\tau) = [12.5 \pm 2.8(\text{stat}) \pm 2.7(\text{syst})] \times 10^{-5}$ [5] reported by Belle in September 2014 is in good agreement with its previous result.

The SM calculation of the leptonic decays suffers from uncertainties in the input values of f_B and V_{ub}. One can eliminate the V_{ub} dependence by calculating the ratio of branching fractions

$$R^\tau_\pi = \frac{\tau_{\bar{B}^0}}{\tau_{B^-}} \frac{\mathcal{B}(B^- \to \tau^- \bar{\nu}_\tau)}{\mathcal{B}(\bar{B}^0 \to \pi^+ \ell^- \bar{\nu}_\ell)}, \tag{1}$$

where $\ell = \mu, e$. The ratio is measured to be (0.73 ± 0.15) [6], which exceeds the SM prediction of $R^\tau_\pi = 0.31 \pm 0.06$ [6] by more than a factor of 2, while the measured value of $\mathcal{B}(\bar{B}^0 \to \pi^+ \ell^- \bar{\nu}_\ell) = (14.6 \pm 0.7) \times 10^{-5}$ [7–9] is consistent with the SM expectation.

The semileptonic decays $B \to D^{(*)} \ell \nu$ have a much richer structure than the leptonic decays. There is a large number of observables in these decays, e.g., the forward-backward asymmetry of the charged lepton. Recently there has been much interest in the ratios of branching fractions

$$R(D^{(*)}) \equiv \frac{\mathcal{B}(\bar{B}^0 \to D^{(*)} \tau^- \bar{\nu}_\tau)}{\mathcal{B}(\bar{B}^0 \to D^{(*)} \ell^- \bar{\nu}_\ell)}. \tag{2}$$

*ivanovm@theor.jinr.ru
†koerner@thep.physik.uni-mainz.de
‡ctt@theor.jinr.ru, tranchienthang1347@gmail.com

In taking these ratios, some of the uncertainties in the form factors are reduced. Furthermore, the dependence on the poorly known CKM matrix element $|V_{cb}|$ drops out in the ratio. Recently, three groups have reported measurements of these ratios[1,10,11]:

$$R(D)|_{\rm BABAR} = 0.440 \pm 0.072, \quad R(D^*)|_{\rm BABAR} = 0.332 \pm 0.030,$$
$$R(D)|_{\rm BELLE} = 0.375 \pm 0.069, \quad R(D^*)|_{\rm BELLE} = 0.293 \pm 0.041,$$
$$R(D^*)|_{\rm LHCb} = 0.336 \pm 0.040,$$

where the statistical and systematic uncertainties have been combined in quadrature. These measurements were combined in [12]

$$R(D)|_{\rm expt} = 0.388 \pm 0.047,$$
$$R(D^*)|_{\rm expt} = 0.321 \pm 0.021 \tag{3}$$

and compared with the SM expectations given in [10,13–15]

$$R(D)|_{\rm SM} = 0.297 \pm 0.017,$$
$$R(D^*)|_{\rm SM} = 0.252 \pm 0.003. \tag{4}$$

It is seen that there is a discrepancy of 1.8σ for $R(D)$ and 3.3σ for $R(D^*)$.

The deviation of leptonic and semileptonic tauonic B-meson decays from SM expectations has been the motivation of many theoretical studies in search for NP effects, including the two-Higgs-doublet models (2HDMs) [16–19], the minimal supersymmetric standard model (MSSM) [20], and leptoquark models [21,22]. In many studies, a general effective Lagrangian for the $b \to u\ell\nu$ and the $b \to c\ell\nu$ transitions in the presence of NP is imposed to investigate various NP operators and their coupling, together with their correlations [14,23–25].

In this paper we focus on these decays within the SM framework, using results from our covariant constituent quark model for the dynamics of the transitions. Most of the theoretical studies on the semileptonic decays have been relying on elements of the heavy quark effective theory (HQET) [26,27], based on a systematic $1/m_Q$ expansion of the QCD Lagrangian. The leading order of the HQET-expansion corresponds to the heavy quark symmetry when the heavy quark mass tends to infinity, simplifying the structure of the weak current transitions. The form factors of these transitions are then expressed through only a few universal functions. Unfortunately, HQET can give predictions only for the normalization of the form factors at zero recoil. As one moves away from the zero-recoil point, one has to take recourse to full nonperturbative calculations. In this paper, we present a description of these decays that does not rely on HQET. We employ the covariant constituent quark model (CQM) with built-in infrared confinement which has been developed in several previous papers by our group (see Refs. [28,29] and references therein). In the CQM approach, the entire physical range of momentum transfer is accessible. This is one of those features that make the CQM different from other model approaches for the calculation of hadronic quantities. We mention that a similar study was done by the authors of Refs. [30–32] in the framework of a relativistic quark model based on the quasipotential approach, in which the full range of momentum transfer is also achievable. Our aim is to give an independent calculation of these decays including the q^2 behavior of the transition form factors, the leptonic decay constants of the B and D mesons, the forward-backward asymmetry of the lepton and other polarization observables, as well as ratios of branching fractions.

II. MODEL

The CQM is based on an effective Lagrangian describing the coupling of a hadron H to its constituent quarks, the coupling strength of which is determined by the compositeness condition $Z_H = 0$ [33,34], where Z_H is the wave function renormalization constant of the hadron H. Here $Z_H^{1/2}$ is the matrix element between a physical particle state and the corresponding bare state. For $Z_H = 0$ it then follows that the physical state does not contain the bare one and is therefore described as a bound state. This does not mean that we can solve the QCD bound state equations, but we are able to show that the compositeness condition provides an effective and self-consistent way to describe the coupling of a particle to its constituents.

One starts with an effective Lagrangian written down in terms of quark and hadron variables [35,36]. Then, by using Feynman rules, the S-matrix elements describing hadronic interactions are derived from a set of quark diagrams. In particular, the compositeness condition enables one to avoid a double counting of hadronic degrees of freedom. This approach is self-consistent, and all calculations of physical observables are straightforward. There is a small set of model parameters: the constituent quark masses, the scale parameters that define the size of the constituent quarks distribution inside a given hadron, and the infrared cutoff parameter λ.

The coupling of a meson M to its constituent quarks q_1 and $\bar{q}_2$ is given by the Lagrangian

$$\mathcal{L}_{\rm int}(x) = g_M M(x) \cdot J_M(x) + {\rm H.c.}, \tag{5}$$

where g_M denotes the coupling strength of the meson with its constituent quarks. The interpolating quark current in (5) is taken to be

$$J_M(x) = \int dx_1 \int dx_2 F_M(x; x_1, x_2) \bar{q}_2(x_2) \Gamma_M q_1(x_1), \quad (6)$$

where the Dirac matrix Γ_M projects onto the relevant meson state, i.e., $\Gamma_M = I$ for a scalar meson, $\Gamma_M = \gamma^5$ for a pseudoscalar meson, and $\Gamma_M = \gamma^\mu$ for a vector meson. The vertex function F_M is related to the scalar part of the Bethe-Salpeter amplitude and characterizes the finite size of the meson. We adopt the following form for the vertex function:

$$F_M(x; x_1, x_2) = \delta(x - w_1 x_1 - w_2 x_2) \Phi_M((x_1 - x_2)^2), \quad (7)$$

where $w_i = m_{q_i}/(m_{q_1} + m_{q_2})$ so that $w_1 + w_2 = 1$. This form of F_M is invariant under the translation $F_M(x + a; x_1 + a, x_2 + a) = F_M(x; x_1, x_2)$, which is a necessary condition to provide the Lorentz invariance of the Lagrangian (5).

In order to simplify the calculations, we adopt a Gaussian form for the vertex function as follows:

$$\tilde{\Phi}_M(-p^2) = \int dx e^{ipx} \Phi_M(x^2) = e^{p^2/\Lambda_M^2}, \quad (8)$$

where the parameter Λ_M characterizes the meson size. Calculations of Feynman diagrams proceed in the Euclidean region where $p^2 = -p_E^2$, in which the vertex function has the appropriate falloff behavior to provide for the ultraviolet convergence of the loop integral.

In the evaluation of the quark-loop diagrams we use the free local fermion propagator of the constituent quark

$$S_q(k) = \frac{1}{m_q - k - i\epsilon} = \frac{m_q + k}{m_q^2 - k^2 - i\epsilon} \quad (9)$$

with an effective constituent quark mass m_q.

For the evaluation of the compositeness condition, we consider the meson mass function defined by the diagram in Fig. 1. One has

$$\tilde{\Pi}_P(p^2) = N_c g_P^2 \int \frac{d^4k}{(2\pi)^4 i} \tilde{\Phi}_P^2(-k^2) \mathrm{tr}(\gamma^5 S_1(k + w_1 p) \times \gamma^5 S_2(k - w_2 p)), \quad (10)$$

$$\tilde{\Pi}_V^{\mu\nu}(p^2) = N_c g_V^2 \int \frac{d^4k}{(2\pi)^4 i} \tilde{\Phi}_V^2(-k^2) \mathrm{tr}(\gamma^\mu S_1(k + w_1 p) \times \gamma^\nu S_2(k - w_2 p)), \quad (11)$$

where $N_c = 3$ is the number of colors. Since the vector meson is on its mass shell, one has $\epsilon_V \cdot p = 0$, and one needs only the part of the vector meson function proportional to $g_{\mu\nu}$. It is given by

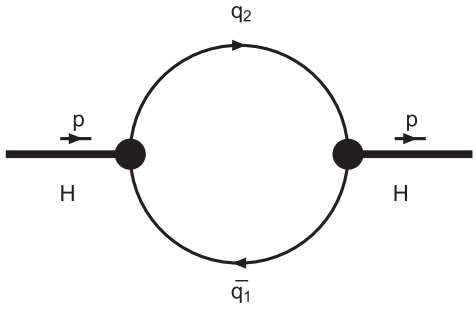

FIG. 1. One-loop self-energy diagram for a meson.

$$\tilde{\Pi}_V(p^2) = \frac{1}{3}\left(g_{\mu\nu} - \frac{p_\mu p_\nu}{p^2}\right)\tilde{\Pi}_V^{\mu\nu}(p). \quad (12)$$

The coupling constant g_M in Eq. (5) is determined by the compositeness condition, which is written in the form

$$Z_M = 1 - \tilde{\Pi}'_M(m_M^2) = 0, \quad (13)$$

where $\tilde{\Pi}'_M(p^2)$ is the derivative of the mass operator taken on the mass shell $p^2 = m_M^2$. It is convenient to calculate the derivatives of the meson mass functions by using the following identities:

$$\frac{d}{dp^2}\tilde{\Pi}_M(p^2) = \frac{1}{2p^2} p^\mu \frac{d}{dp^\mu}\tilde{\Pi}_M(p^2),$$
$$p^\mu \frac{d}{dp^\mu} S(k + wp) = wS(k + wp)\not{p}S(k + wp). \quad (14)$$

Accordingly, the derivatives of the meson mass functions can be written as

$$\tilde{\Pi}'_P(p^2) = \frac{1}{2p^2}\frac{3g_P^2}{4\pi^2}\int \frac{dk}{4\pi^2 i}\tilde{\Phi}_P^2(-k^2) \times \{w_1 \mathrm{tr}[S_1(k + w_1 p)\not{p}S_1(k + w_1 p)\gamma^5 S_2(k - w_2 p)\gamma^5] - w_2 \mathrm{tr}[S_1(k + w_1 p)\gamma^5 S_2(k - w_2 p)\not{p}S_2(k - w_2 p)\gamma^5]\}, \quad (15)$$

$$\tilde{\Pi}'_V(p^2) = \frac{1}{2p^2}\frac{1}{3}\left(g^{\mu\nu} - \frac{p^\mu p^\nu}{p^2}\right)\frac{3g_V^2}{4\pi^2}\int \frac{dk}{4\pi^2 i}\tilde{\Phi}_V^2(-k^2) \times \{w_1 \mathrm{tr}[S_1(k + w_1 p)\not{p}S_1(k + w_1 p)\gamma_\mu S_2(k - w_2 p)\gamma_\nu] - w_2 \mathrm{tr}[S_1(k + w_1 p)\gamma_\mu S_2(k - w_2 p)\not{p}S_2(k - w_2 p)\gamma_\nu]\}. \quad (16)$$

The loop integrations in Eqs. (15) and (16) are done with the help of the Fock-Schwinger representation of quark propagators:

$$S_q(k+wp) = \frac{1}{m_q - \not{k} - w\not{p}} = \frac{m_q + \not{k} + w\not{p}}{m_q^2 - (k+wp)^2} = (m_q + \not{k} + w\not{p}) \int_0^\infty d\alpha e^{-\alpha[m_q^2 - (k+wp)^2]}. \tag{17}$$

As will be described later, the use of the Fock-Schwinger representation allows one to do tensor loop integrals in a very efficient way, since one can convert loop momenta into derivatives of the exponent function (see, e.g., Refs. [37–39]).

As mentioned above, all loop integrations are carried out in Euclidean space. The transition from Minkowski space to Euclidean space is performed by using the Wick rotation

$$k_0 = e^{i\frac{\pi}{2}} k_4 = ik_4 \tag{18}$$

so that $k^2 = k_0^2 - \vec{k}^2 = -k_4^2 - \vec{k}^2 = -k_E^2 \le 0$. Simultaneously, one has to rotate all external momenta, i.e. $p_0 \to ip_4$, so that $p^2 = -p_E^2 \le 0$. Then the quadratic form in Eq. (17) becomes positive definite,

$$m_q^2 - (k+wp)^2 = m_q^2 + (k_E + wp_E)^2 > 0,$$

and the integral over α is absolutely convergent. We will keep the Minkowski notation to avoid excessive relabeling. We simply imply that $k^2 \le 0$ and $p^2 \le 0$.

Collecting the representations of the vertex functions and quark propagators given by Eqs. (8) and (17), respectively, one can perform the Gaussian integration in the derivatives of the mass functions in Eqs. (10) and (11). The exponent has the form $ak^2 + 2kr + z_0$, where $r = bp$. Using the properties (where k is the loop momentum)

$$\left.\begin{aligned} k^\mu \exp(ak^2 + 2kr + z_0) &= \tfrac{1}{2}\tfrac{\partial}{\partial r_\mu} \exp(ak^2 + 2kr + z_0) \\ k^\mu k^\nu \exp(ak^2 + 2kr + z_0) &= \tfrac{1}{2}\tfrac{\partial}{\partial r_\mu}\tfrac{1}{2}\tfrac{\partial}{\partial r_\nu} \exp(ak^2 + 2kr + z_0) \\ &\text{etc.} \end{aligned}\right\}, \tag{19}$$

one can replace $\not{k}$ with $\not{\partial}_r = \gamma^\mu \frac{\partial}{\partial r_\mu}$ which allows one to exchange the tensor integrations for a differentiation of the Gaussian exponent. For example, Eq. (10) now has the form

$$\tilde{\Pi}_P(p^2) = \frac{3g_P^2}{16\pi^2} \int_0^\infty \int_0^\infty \frac{d\alpha_1 d\alpha_2}{a^2} \times \mathrm{tr}[\gamma^5 (m_1 + \not{\partial}_r + w_1\not{p})\gamma^5 (m_2 + \not{\partial}_r - w_2\not{p})] e^{-\frac{r^2}{a} + z_0}. \tag{20}$$

The r-dependent Gaussian exponent $e^{-r^2/a}$ can be moved to the left through the differential operator ∂_r by using the following properties:

$$\frac{\partial}{\partial r_\mu} e^{-r^2/a} = e^{-r^2/a}\left[-\frac{2r^\mu}{a} + \frac{\partial}{\partial r_\mu}\right],$$
$$\frac{\partial}{\partial r_\mu}\frac{\partial}{\partial r_\nu} e^{-r^2/a} = e^{-r^2/a}\left[-\frac{2r^\mu}{a} + \frac{\partial}{\partial r_\mu}\right]\cdot\left[-\frac{2r^\nu}{a} + \frac{\partial}{\partial r_\nu}\right], \text{etc.} \tag{21}$$

Finally, one has to move the derivatives to the right by using the commutation relation

$$\left[\frac{\partial}{\partial r_\mu}, r^\nu\right] = g^{\mu\nu}. \tag{22}$$

The last step has been done by using a FORM code which works for any numbers of loops and propagators. In the remaining integrals over the Fock-Schwinger parameters $0 \le \alpha_i < \infty$, we introduce an additional integration which converts the set of Fock-Schwinger parameters into a simplex. Using the transformation

$$\prod_{i=1}^n \int_0^\infty d\alpha_i f(\alpha_1, \ldots, \alpha_n) = \int_0^\infty dt t^{n-1} \prod_{i=1}^n \int d\alpha_i \delta\left(1 - \sum_{i=1}^n \alpha_i\right) f(t\alpha_1, \ldots, t\alpha_n), \tag{23}$$

one finds

$$\begin{aligned} \tilde{\Pi}'_M(p^2) &= \frac{3g_M^2}{4\pi^2} \int_0^\infty \frac{dtt}{a_M^2} \int_0^1 d\alpha e^{-tz_0 + z_M} f_M(t,\alpha), \\ z_0 &= \alpha m_{q_1}^2 + (1-\alpha)m_{q_2}^2 - \alpha(1-\alpha)p^2, \\ z_M &= \frac{2s_M t}{2s_M + t}(\alpha - w_2)^2 p^2, \\ a_M &= 2s_M + t, b = (\alpha - w_2)t. \end{aligned} \tag{24}$$

The function $f_M(t,\alpha)$ arises from the trace evaluation. Further, we have introduced the parameter $s_M = 1/\Lambda_M^2$.

It is readily seen that the integral over t in Eq. (24) is well defined and convergent if $z_0 > 0$, i.e. below the threshold $p^2 < (m_{q_1} + m_{q_2})^2$. The convergence of the integral in the case of negative values of $z_0 \le 0$, i.e. above threshold $p^2 \ge (m_{q_1} + m_{q_2})^2$, is guaranteed by the addition of a small imaginary to the quark mass, i.e. $m_q \to m_q - i\epsilon$, $\epsilon > 0$ in the quark propagator Eq. (9). It allows one to rotate the integration variable t to the imaginary axis $t \to it$. As a result, the integral Eq. (24) becomes convergent but obtains an imaginary part corresponding to quark pair production.

However, by cutting the scale integration at the upper limit corresponding to the introduction of an infrared cutoff

$$\int_0^\infty dt(\ldots) \to \int_0^{1/\lambda^2} dt(\ldots), \tag{25}$$

one can remove all possible thresholds present in the initial quark diagram [28]. Thus the infrared cutoff parameter λ effectively guarantees the confinement of quarks within hadrons. This method is quite general and can be used for diagrams with an arbitrary number of loops and propagators. In the CQM, the infrared cutoff parameter λ is taken to be universal for all physical processes.

III. LEPTONIC B-MESON DECAYS

The model parameters are determined by fitting calculated quantities of basic processes to available experimental data or lattice simulations (for details, see Ref. [28], where a different set of weak and electromagnetic decays has been used). In this paper we will use the updated least-squares fit performed in Refs. [40–42]. In this fit we have also updated some of the theoretical/experimental input values. The infrared cutoff parameter λ of the model has been kept fixed. The numerical values of the constituent quark masses and the parameter λ are given by (all in GeV)

m_u	m_s	m_c	m_b	λ
0.241	0.428	1.67	5.04	0.181

. (26)

Our prime goal is to study the pure leptonic B-meson decays as well as the semileptonic $B \to D^{(*)}\ell\bar{\nu}_\ell$ decays. The most recent results of the fit for those parameters involved in this paper are taken from our papers, Refs. [40–42] (all in GeV):

Λ_{D^*}	$\Lambda_{D_s^*}$	Λ_D	Λ_{D_s}	$\Lambda_{B_s^*}$	Λ_{B^*}	Λ_B	Λ_{B_s}	Λ_{B_c}
1.53	1.56	1.60	1.75	1.79	1.81	1.96	2.05	2.73

. (27)

The matrix elements of the leptonic decays are described by the Feynman diagram shown in Fig. 2. The leptonic decay constants of the pseudoscalar and vector mesons are defined by

$$\begin{aligned} &N_c g_P \int \frac{d^4k}{(2\pi)^4 i} \tilde{\Phi}_P(-k^2)\mathrm{tr}[O^\mu S_1(k+w_1 p)\gamma^5 S_2(k-w_2 p)] \\ &\quad = f_P p^\mu, \\ &N_c g_V \int \frac{d^4k}{(2\pi)^4 i} \tilde{\Phi}_V(-k^2)\mathrm{tr}[O^\mu S_1(k+w_1 p)\epsilon\!\!\!/_V S_2(k-w_2 p)] \\ &\quad = m_V f_V \epsilon_V^\mu, \end{aligned} \tag{28}$$

where $N_c = 3$ is the number of colors, and $O^\mu = \gamma^\mu(1-\gamma_5)$ is the weak Dirac matrix with left chirality. The mesons are taken on their mass shells. The calculation of the matrix elements (28) proceeds in a way similar to the case of the mass functions.

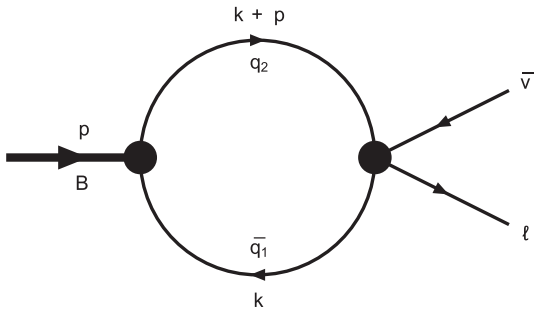

FIG. 2. Quark model diagram for the B-meson leptonic decay.

Our results for the leptonic decay constants of $B_{(s)}^{(*)}$ and $D_{(s)}^{(*)}$ mesons are given in Table I. For comparison, we also list the values of these constants obtained from experiments, lattice, and QCD sum rules. Our results show good agreement (within 10%) with results of the other studies. We mention that early attempts to account for flavor symmetry breaking in pseudoscalar meson decay constants were made in Refs. [43,44].

In the SM, the purely leptonic decays $B^- \to \ell^-\bar{\nu}_\ell$ proceed via the annihilation of the quark pair into an off-shell W boson. The branching fraction for the leptonic decays is given by

TABLE I. Results for the leptonic decay constants f_H (in MeV).

	This work	Other	Reference
f_B	193.1	190.6 ± 4.7	PDG [45]
f_{B_s}	238.7	242.0(9.5)	LAT [46]
		259(32)	HPQCD LAT [47]
		193(7)	LAT [48]
f_{B_c}	489.0	$489 \pm 4 \pm 3$	LAT [49]
f_{B^*}	196.0	$196(24)^{+39}_{-2}$	LAT [50]
		186.4 ± 3.2	QCDSR [51]
$f_{B_s^*}$	229.0	$229(20)^{+41}_{-16}$	LAT [50]
		215.2 ± 3.0	QCD SR [51]
f_{B_s}/f_B	1.236	1.20(3)(1)	HPQCD LAT [47]
		1.229(26)	LAT [46]
f_D	206.1	204.6 ± 5.0	PDG [45]
f_{D^*}	244.3	$278 \pm 13 \pm 10$	LAT [52]
		$245(20)^{+3}_{-2}$	LAT [50]
		$252.2 \pm 22.3 \pm 4$	QCD SR [53]
f_{D_s}	257.5	257.5 ± 4.6	PDG [45]
$f_{D_s^*}$	272.0	311 ± 9	LAT [52]
		$272(16)^{+3}_{-20}$	LAT [50]
		$305.5 \pm 26.8 \pm 5$	QCD SR [53]
f_{D_s}/f_D	1.249	1.258 ± 0.038	PDG [45]

$$\mathcal{B}(B^- \to \ell^- \bar{\nu}_\ell) = \frac{G_F^2}{8\pi} m_B m_\ell^2 \left(1 - \frac{m_\ell^2}{m_B^2}\right)^2 f_B^2 |V_{ub}|^2 \tau_B, \quad (29)$$

where G_F is the Fermi coupling constant, m_B and m_ℓ are the B-meson and lepton masses, respectively, and τ_B is the B-meson lifetime. The expected branching fractions are $O(10^{-4})$, $O(10^{-7})$, and $O(10^{-11})$ for $\ell = \tau, \mu$, and e, respectively. The different lepton masses affect the values of the branching fractions through the helicity flip factor $(1 - m_\ell^2/m_B^2)^2$.

IV. FORM FACTORS OF SEMILEPTONIC B-MESON DECAYS

The invariant matrix element of the semileptonic decays $B \to D^{(*)} \ell^- \bar{\nu}_\ell$ can be written as

$$M(B \to D^{(*)} \ell^- \bar{\nu}_\ell) = \frac{G_F}{\sqrt{2}} V_{cb} < D^{(*)} | \bar{c} O^\mu b | B > \bar{\ell} O_\mu \nu_\ell, \quad (30)$$

where the matrix elements of the semileptonic $B \to D^{(*)}$ transitions in the covariant quark model are defined by the diagram in Fig. 3 and are written as

$$\begin{aligned} T^\mu &\equiv \langle D(p_2) | \bar{c} O^\mu b | B(p_1) \rangle \\ &= N_c g_B g_D \int \frac{d^4k}{(2\pi)^4 i} \tilde{\Phi}_B(-(k + w_{13} p_1)^2) \\ &\quad \times \tilde{\Phi}_D(-(k + w_{23} p_2)^2) \\ &\quad \times \mathrm{tr}[O^\mu S_1(k + p_1) \gamma^5 S_3(k) \gamma^5 S_2(k + p_2)] \\ &= F_+(q^2) P^\mu + F_-(q^2) q^\mu, \quad \text{and} \end{aligned} \quad (31)$$

$$\begin{aligned} \epsilon_{2\alpha}^\dagger T^{\mu\alpha} &\equiv \langle D^*(p_2, \epsilon_2) | \bar{c} O^\mu b | B(p_1) \rangle \\ &= N_c g_B g_{D^*} \int \frac{d^4k}{(2\pi)^4 i} \tilde{\Phi}_B(-(k + w_{13} p_1)^2) \\ &\quad \times \tilde{\Phi}_{D^*}(-(k + w_{23} p_2)^2) \\ &\quad \times \mathrm{tr}[O^\mu S_1(k + p_1) \gamma^5 S_3(k) \epsilon_2^\dagger S_2(k + p_2)] \\ &= \frac{\epsilon_{2\alpha}^\dagger}{m_1 + m_2} (-g^{\mu\alpha} Pq A_0(q^2) + P^\mu P^\alpha A_+(q^2) \\ &\quad + q^\mu P^\alpha A_-(q^2) + i\varepsilon^{\mu\alpha Pq} V(q^2)). \end{aligned} \quad (32)$$

Here, $P = p_1 + p_2$, $q = p_1 - p_2$, and ϵ_2 is the polarization vector of the D^* meson, so that $\epsilon_2^\dagger \cdot p_2 = 0$. The particles are on their mass shells: $p_1^2 = m_1^2 = m_B^2$ and $p_2^2 = m_2^2 = m_{D^{(*)}}^2$. Altogether there are three flavors of quarks involved in these processes. We therefore introduce a notation with two subscripts $w_{ij} = m_{q_j}/(m_{q_i} + m_{q_j})$ $(i, j = 1, 2, 3)$ such that $w_{ij} + w_{ji} = 1$. In our case, one has $q_1 = b$, $q_2 = c$, and $q_3 = d$.

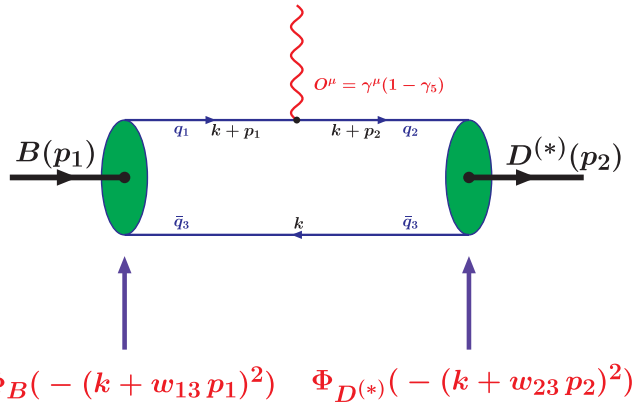

FIG. 3 (color online). Quark model diagram for B-meson semileptonic decay.

Our numerical results for the form factors are well represented by a double-pole parametrization

$$F(q^2) = \frac{F(0)}{1 - as + bs^2}, \qquad s = \frac{q^2}{m_1^2}. \quad (33)$$

The double-pole approximation is quite accurate. The error relative to the exact results is less than 1% over the entire q^2 range. For the $B \to D^{(*)}$ transition, the parameters of the dipole approximation are given by

	F_+	F_-	A_0	A_+	A_-	V
$F(0)$	0.78	−0.36	1.62	0.67	−0.77	0.77
a	0.74	0.76	0.34	0.87	0.89	0.90
b	0.038	0.046	−0.16	0.057	0.070	0.075.

(34)

Since b/a is quite small for the form factors F_+, F_-, A_+, A_-, and V, these form factors show a monopole-like falloff behavior, whereas A_0 has a substantial $(q^2)^{-2}$ contribution. In Fig. 4 we present our results for the semileptonic form factors within the full range of momentum transfer $0 \le q^2 \le q^2_{\max}$, where $q^2_{\max} = (m_B - m_{D^{(*)}})^2$. The results of the exact calculations are shown by solid lines, whereas the results obtained in the heavy quark limit are shown by dashed lines. We will discuss the heavy quark limit in the next section. It is interesting to note that the QCD counting rules prescribe a $(q^2)^{-1}$ and a $(q^2)^{-2}$ falloff behavior for the form factors F_+, F_-, A_0 and A_+, A_-, V, respectively.

As recently noticed in Ref. [54], the ratio $F_0(q^2)/F_+(q^2)$ exhibits a linear q^2 behavior

$$F_0(q^2) = F_+(q^2) + \frac{q^2}{Pq} F_-(q^2), \quad \frac{F_0(q^2)}{F_+(q^2)} = 1 - \alpha q^2, \quad (35)$$

where the slope $\alpha = 0.020(1)\ \mathrm{GeV}^{-2}$ was determined precisely based on lattice values of the two form factors.

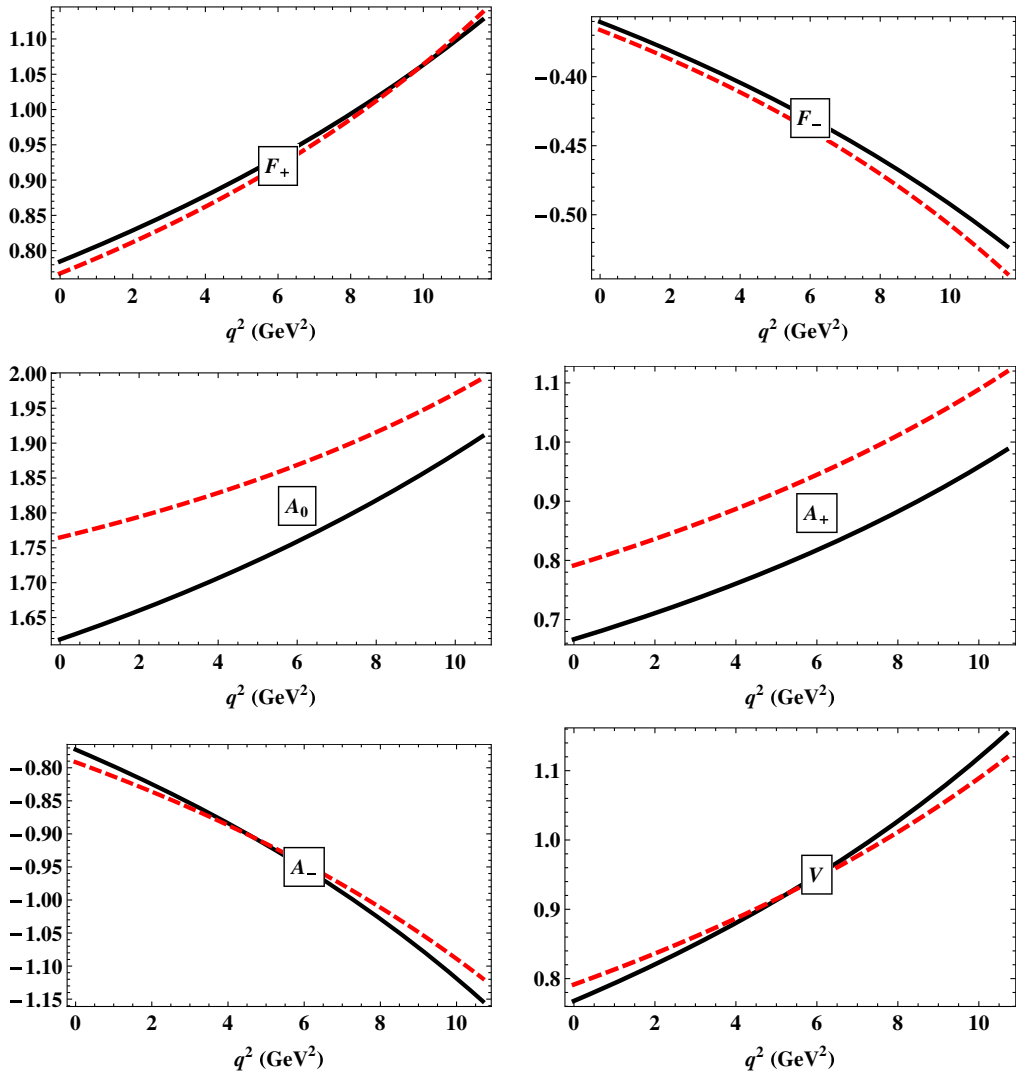

FIG. 4 (color online). Form factors of the decays $B \to D^{(*)}\ell\nu$. The solid lines are the results of exact calculations in our approach; the dashed lines are the form factors obtained in the heavy quark limit.

We also plot the q^2 dependence of the ratio $F_0(q^2)/F_+(q^2)$ in Fig. 5, which shows a linear behavior as mentioned. Our value for the slope is $\alpha = 0.019$ GeV^{-2}, which very well agrees with the lattice result.

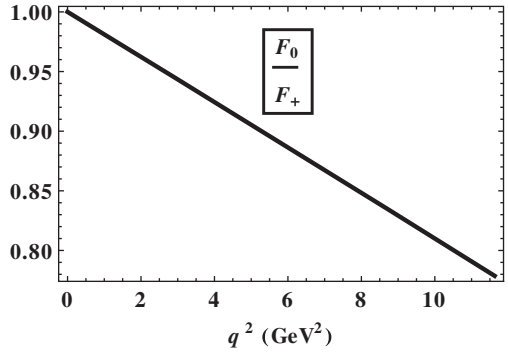

FIG. 5. Ratio $F_0(q^2)/F_+(q^2)$.

V. HEAVY QUARK LIMIT

It is instructive to explore the heavy quark limit (HQL) in the heavy-to-heavy transition $B \to D(D^*)$. In the HQL, one takes the limit $m_B = m_b + E$, $m_b \to \infty$ and $m_D = m_{D^*} = m_c + E$, $m_c \to \infty$ in the expressions for the coupling constants and form factors. In this limit the heavy quark propagators are reduced to the static form

$$S_b(k+p_1) = \frac{1}{m_b - k - \not{p}_1} \to \frac{1+\not{v}_1}{-2kv_1 - 2E} + O\left(\frac{1}{m_b}\right),$$
$$S_c(k+p_2) = \frac{1}{m_c - k - \not{p}_2} \to \frac{1+\not{v}_2}{-2kv_2 - 2E} + O\left(\frac{1}{m_c}\right), \tag{36}$$

where p_i and $v_i = p_i/m_i$ $(i = 1, 2)$ are the momenta and the four-velocities of the initial and final states. Moreover, we have to keep the size parameters of heavy hadrons equal

to each other in order to provide the correct normalization of the Isgur-Wise function at zero recoil. By using the technique developed in our previous papers—see, for instance, Refs. [55,56]—one can arrive at the following expressions for the semileptonic heavy-to-heavy transitions defined by Eqs. (31) and (32):

$$T^{\mu}_{\rm HQL} = \xi(w)\cdot\frac{1}{4}{\rm tr}[O^{\mu}(1+\not{v}_1)\gamma^5\cdot\gamma^5(1+\not{v}_2)] = \xi(w)\cdot(v_1^{\mu}+v_2^{\mu}), \tag{37}$$

$$\epsilon^{\dagger}_{2\nu}T^{\mu\nu}_{\rm HQL} = \xi(w)\cdot\frac{1}{4}{\rm tr}[O^{\mu}(1+\not{v}_1)\gamma^5\cdot\not{\epsilon}^{\dagger}_2(1+\not{v}_2)] = \xi(w)\cdot\epsilon^{\dagger}_{2\nu}(-g^{\mu\nu}(1+w)+v_1^{\mu}v_2^{\nu}+v_1^{\nu}v_2^{\mu}-i\epsilon^{\mu\nu v_1 v_2}). \tag{38}$$

Here, $w = v_1 v_2$, and the Isgur-Wise function is equal to

$$\xi(w) = \frac{J_3(E,w)}{J_3(E,1)},$$
$$J_3(E,w) = \int_0^1 \frac{d\tau}{W}\int_0^{\infty} du\tilde{\Phi}^2(z)\left(\sigma_S(z)+\sqrt{\frac{u}{W}}\sigma_V(z)\right), \tag{39}$$

where $W = 1+2\tau(1-\tau)(w-1)$, $z = u - 2E\sqrt{u/W}$, and

$$\tilde{\Phi}(z) = \exp(-z/\Lambda^2),$$
$$\sigma_S(z) = \frac{m_u}{m_u^2+z},$$
$$\sigma_V(z) = \frac{1}{m_u^2+z}.$$

By using the definition of the form factors given by Eqs. (31) and (32), one can easily obtain the expressions of the form factors in the HQL. One finds

$$F_{\pm}(q^2) = \pm\frac{m_1\pm m_2}{2\sqrt{m_1 m_2}}\xi(w),$$
$$A_0(q^2) = \frac{\sqrt{m_1 m_2}}{m_1-m_2}(1+w)\xi(w),$$
$$A_+(q^2) = -A_-(q^2) = V(q^2) = \frac{m_1+m_2}{2\sqrt{m_1 m_2}}\xi(w), \tag{40}$$

where $w = (m_1^2+m_2^2-q^2)/(2m_1m_2)$. We use the physical masses of the heavy hadrons in the numerical calculations. For the size parameter we adopt the average value $\Lambda = (\Lambda_B+\Lambda_D+\Lambda_{D^*})/3 = 1.70$ GeV. The parameter E characterizes the difference in mass between the heavy hadron and the corresponding heavy quark. We use its minimal value $E = m_D - m_c = 0.20$ GeV in order to avoid the complication with confinement.

In Fig. 4 we display the heavy-to-heavy transition form factors calculated in the HQL and compare them with the results of exact calculations. One can see that the two results obtained with and without use of the HQL behave very similar to each other, which demonstrates the fidelity of HQET.

One can also consider the near zero-recoil behavior of the form factors in a similar way as we did in our paper on the semileptonic decay $\Lambda_b \to \Lambda_c + \tau\bar{\nu}_{\tau}$ [40]. The standard parametrization of the $(w-1)$ expansion takes the form

$$F(q^2(w)) = F(q^2_{\rm max})[1-\rho^2(w-1)+c(w-1)^2+\cdots],$$

where ρ^2 is called the slope parameter and c the convexity parameter. The numerical results are given below:

	F_+	F_-	A_0	A_+	A_-	V
$F(q^2_{\rm max})$	1.12	−0.52	1.91	0.99	−1.15	1.16
ρ^2	0.72	0.74	0.42	0.93	0.95	0.96
c	0.49	0.51	0.28	0.82	0.85	0.86

(41)

which may be compared with the results obtained for the monopole form factor of a B_c-resonance contribution: $\rho^2 = 0.71$ and $c = 0.51$.

It is interesting to compare the zero-recoil values of our exact form factors with the predictions of leading-order HQET at $w = 1$ where $\xi(1) = 1$. One has

$$F_+ = \frac{m_1+m_2}{2\sqrt{m_1m_2}} = 1.138, \qquad F_- = -\frac{m_1-m_2}{2\sqrt{m_1m_2}} = -0.543,$$
$$A_+ = -A_- = V = \frac{m_1+m_2}{2\sqrt{m_1m_2}} = 1.119,$$
$$A_0 = \frac{2\sqrt{m_1m_2}}{m_1-m_2} = 1.993. \tag{42}$$

The zero-recoil values of our model form factors can be seen to be quite close to the corresponding HQET values, except for the form factor A_+, where our form factor value exceeds the HQET result by ∼13%.

VI. HELICITY AMPLITUDES AND TWO-FOLD DISTRIBUTIONS

Let us first consider the polar angle differential decay distribution in the momentum transfer squared, q^2. The polar angle is defined by the angle between $\vec{q} = \vec{p}_1 - \vec{p}_2$ and the three-momentum of the charged lepton $\vec{k}_1$ in the $(\ell^-\bar{\nu}_{\ell})$ rest frame as shown in Fig. 6. One has

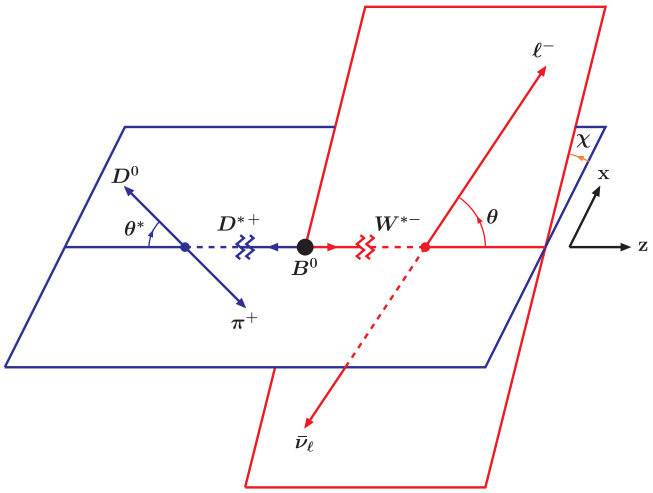

FIG. 6 (color online). Definition of angles θ, θ^*, and χ in the cascade decay $\bar{B}^0 \to D^{*+}(\to D^0\pi^+)\ell^-\bar{\nu}_\ell$.

$$\frac{d^2\Gamma}{dq^2 d\cos\theta} = \frac{|\mathbf{p_2}|v}{(2\pi)^3 32 m_1^2}\cdot\sum_{\text{pol}}|M|^2 = \frac{G_F^2}{(2\pi)^3}|V_{cb}|^2\frac{|\mathbf{p_2}|v}{64m_1^2}H^{\mu\nu}L_{\mu\nu}, \tag{43}$$

where $|\mathbf{p_2}| = \lambda^{1/2}(m_1^2, m_2^2, q^2)/2m_1$ is the momentum of the daughter meson and where we have introduced the velocity-type parameter $v = 1 - m_\ell^2/q^2$, as well as the contraction of hadron and lepton tensors $H^{\mu\nu}L_{\mu\nu}$.

As discussed in some detail in Ref. [40], the covariant contraction $H^{\mu\nu}L_{\mu\nu}$ can be converted to a sum of bilinear products of hadronic and leptonic helicity amplitudes using the completeness relation for the polarization four-vectors of the process. A synopsis of the necessary steps in this transformation is provided in the Appendix.

One needs to relate the mesonic helicity amplitudes to the invariant form factors defined in Eqs. (31) and (32). To do so, one requires explicit representations of the polarization four-vectors $\epsilon^\mu(\lambda_W)$. They read

$$\begin{aligned}\epsilon^\mu(t) &= \frac{1}{\sqrt{q^2}}(q_0, 0, 0, |\mathbf{p_2}|),\\ \epsilon^\mu(\pm) &= \frac{1}{\sqrt{2}}(0, \mp 1, -i, 0),\\ \epsilon^\mu(0) &= \frac{1}{\sqrt{q^2}}(|\mathbf{p_2}|, 0, 0, q_0).\end{aligned} \tag{44}$$

The linear relations between the two sets of form factors can then be calculated in the following way.

A. $B \to D$ transition:

The helicity amplitudes are defined by $H_{\lambda_W} = \epsilon^{\dagger\mu}(\lambda_W)T_\mu$. One obtains

$$H_t = \frac{1}{\sqrt{q^2}}(PqF_+ + q^2F_-), \quad H_\pm = 0, \quad H_0 = \frac{2m_1|\mathbf{p_2}|}{\sqrt{q^2}}F_+. \tag{45}$$

Note the zero-recoil relation $H_0 = 0$. At the other end of the spectrum, at maximal recoil $q^2 = 0$, one has $H_t = H_0$. In the Appendix we describe how to obtain the differential $(q^2, \cos\theta)$ distribution. One has

$$\begin{aligned}&\frac{d\Gamma(B \to D\ell^-\bar{\nu}_\ell)}{dq^2 d\cos\theta}\\ &= \frac{G_F^2|V_{cb}|^2|\mathbf{p_2}|q^2v^2}{32(2\pi)^3 m_1^2}\\ &\quad\times\{2\sin^2\theta\mathcal{H}_L + 2\delta_\ell(2\cos^2\theta\mathcal{H}_L + 2\mathcal{H}_S - 4\cos\theta\mathcal{H}_{SL})\},\end{aligned} \tag{46}$$

where we have introduced the helicity flip penalty factor $\delta_\ell = m_\ell^2/2q^2$ and the helicity structure functions $\mathcal{H}_L = |H_0|^2$, $\mathcal{H}_S = |H_t|^2$, and $\mathcal{H}_{SL} = \text{Re}(H_0H_t^\dagger)$.

B. $B \to D^*$ transition:

The helicity amplitudes are defined by $H_{\lambda_W\lambda_{D^*}} = \epsilon^{\dagger\mu}(\lambda_W)\epsilon_2^{\dagger\alpha}(\lambda_{D^*})T_{\mu\alpha}$. In addition to the $W_{\text{off-shell}}$ polarization four-vectors $\epsilon^\mu(\lambda_W)$, one needs the polarization four-vectors $\epsilon_2^\alpha(\lambda_{D^*})$ of the D^*. They read ($E_2 = m_1 - q_0$)

$$\begin{aligned}\epsilon_2^\alpha(\pm) &= \frac{1}{\sqrt{2}}(0, \pm 1, -i, 0),\\ \epsilon_2^\alpha(0) &= \frac{1}{m_2}(|\mathbf{p_2}|, 0, 0, -E_2).\end{aligned} \tag{47}$$

One obtains

$$\begin{aligned}H_{t0} &= \epsilon^{\dagger\mu}(t)\epsilon_2^{\dagger\alpha}(0)T_{\mu\alpha}\\ &= \frac{1}{m_1+m_2}\frac{m_1|\mathbf{p_2}|}{m_2\sqrt{q^2}}(Pq(-A_0 + A_+) + q^2A_-),\\ H_{\pm1\pm1} &= \epsilon^{\dagger\mu}(\pm)\epsilon_2^{\dagger\alpha}(\pm)T_{\mu\alpha}\\ &= \frac{1}{m_1+m_2}(-PqA_0 \pm 2m_1|\mathbf{p_2}|V),\\ H_{00} &= \epsilon^{\dagger\mu}(0)\epsilon_2^{\dagger\alpha}(0)T_{\mu\alpha}\\ &= \frac{1}{m_1+m_2}\frac{1}{2m_2\sqrt{q^2}}\\ &\quad\times(-Pq(m_1^2 - m_2^2 - q^2)A_0 + 4m_1^2|\mathbf{p_2}|^2A_+).\end{aligned} \tag{48}$$

Note the zero-recoil relations $H_{t0} = 0$ and $H_{\pm1\pm1} = H_{00}$. At maximal recoil $q^2 = 0$, the dominating helicity amplitudes are H_{t0} and H_{00} with $H_{t0} = H_{00}$.

The differential $(q^2, \cos\theta)$ distribution finally reads (see the Appendix)

$$\frac{d\Gamma(B\to D^*\ell^-\bar\nu_\ell)}{dq^2 d(\cos\theta)} = \frac{G_F^2|V_{cb}|^2|\mathbf{p_2}|q^2v^2}{32(2\pi)^3 m_1^2}\{(1+\cos^2\theta)\mathcal{H}_U + 2\sin^2\theta\mathcal{H}_L - 2\cos\theta\mathcal{H}_P + 2\delta_\ell(\sin^2\theta\mathcal{H}_U + 2\cos^2\theta\mathcal{H}_L + 2\mathcal{H}_S - 4\cos\theta\mathcal{H}_{SL})\}. \quad (49)$$

The relevant bilinear combinations of the helicity amplitudes are defined in Table II. We have dropped a factor of 3 in the definition of $\mathcal{H}_S$ and $\mathcal{H}_{IS}$ compared to our paper [57]. Note that the helicity structure functions satisfy the zero-recoil relations $2\mathcal{H}_U = \mathcal{H}_L = \mathcal{H}_T = \mathcal{H}_I$ and $\mathcal{H}_P = \mathcal{H}_A = \mathcal{H}_S = \mathcal{H}_{SA} = \mathcal{H}_{ST} = \mathcal{H}_S = 0$. Similar relations hold for the imaginary parts. At maximal recoil, one has $\mathcal{H}_L = \mathcal{H}_S = \mathcal{H}_{SL}$ for the dominating helicity structure functions.

Let us begin discussing the $\cos\theta$ distribution for the $B\to D^*\ell^-\bar\nu_\ell$ case. The distribution (46) is described by a tilted parabola whose normalized form reads

$$\widetilde{W}(\theta) = \frac{a + b\cos\theta + c\cos^2\theta}{2(a+c/3)}. \quad (50)$$

The linear coefficient $b/2(a+c/3)$ can be projected out by defining a forward-backward asymmetry given by [58]

$$\mathcal{A}_{FB}(q^2) = \frac{d\Gamma(F) - d\Gamma(B)}{d\Gamma(F) + d\Gamma(B)} = \frac{\int_0^1 d\cos\theta d\Gamma/d\cos\theta - \int_{-1}^0 d\cos\theta d\Gamma/d\cos\theta}{\int_0^1 d\cos\theta d\Gamma/d\cos\theta + \int_{-1}^0 d\cos\theta d\Gamma/d\cos\theta} = \frac{b}{2(a+c/3)} = -\frac{3}{4}\frac{\mathcal{H}_P + 4\delta_\ell\mathcal{H}_{SL}}{\mathcal{H}_{\rm tot}}. \quad (51)$$

In the τ mode there are two sources of the parity-odd forward-backward asymmetry, namely a purely parity-violating source from the VA interaction leading to the $\mathcal{H}_P$ contribution, and a parity-conserving source from the VV and AA interactions leading to the $\mathcal{H}_{SL}$ contribution. The parity-conserving parity-odd contribution $\mathcal{H}_{SL}$ arises from the interference of the $(0^+;1^-)$ and $(0^-;1^+)$ components of the VV and AA products of currents, respectively. In the case of the $B\to D$ transition, the forward-backward asymmetry arises solely from the $(0^+;1^-)$ interference term of the VV product of currents.

The coefficient $c/2(a+c/3)$ of the quadratic contribution is obtained by taking the second derivative of $\tilde W(\theta)$. Accordingly, we define a convexity parameter by writing

$$C_F^\ell(q^2) = \frac{d^2\widetilde{W}(\theta)}{d(\cos\theta)^2} = \frac{c}{a+c/3} = \frac{3}{4}(1-2\delta_\ell)\frac{\mathcal{H}_U - 2\mathcal{H}_L}{\mathcal{H}_{\rm tot}}. \quad (52)$$

When calculating the q^2 averages of the forward-backward asymmetry and the convexity parameter, one has to multiply the numerator and denominator of (51) and (52) by the q^2-dependent piece of the phase-space factor in (46) given by $C(q^2) = |\mathbf{p_2}|q^2v^2$. For example, the mean forward-backward asymmetry can then be calculated according to

$$\langle\mathcal{A}_{FB}\rangle = -\frac{3}{4}\frac{\int dq^2 C(q^2)(\mathcal{H}_P + 4\delta_\ell\mathcal{H}_{SL})}{\int dq^2 C(q^2)\mathcal{H}_{\rm tot}}. \quad (53)$$

Finally, integrating Eq. (46) over $\cos\theta$, one obtains

$$\frac{d\Gamma(B\to D^{(*)}\ell^-\bar\nu_\ell)}{dq^2} = \frac{G_F^2|V_{cb}|^2|\mathbf{p_2}|q^2v^2}{12(2\pi)^3 m_1^2}\cdot\mathcal{H}_{\rm tot}, \quad (54)$$

where $\mathcal{H}_{\rm tot} = \mathcal{H}_U + \mathcal{H}_L + \delta_\ell(\mathcal{H}_U + \mathcal{H}_L + 3\mathcal{H}_S)$.

The discussion of the $\cos\theta$ distribution for the $B\to D\ell^-\bar\nu_\ell$ case proceeds in a similar way, except that one has to drop the contributions of the helicity structure functions $\mathcal{H}_U$ and $\mathcal{H}_P$.

VII. FOUR-FOLD ANGULAR DECAY DISTRIBUTION

The lepton-hadron correlation function $L_{\mu\nu}H^{\mu\nu}$ reveals even more structures when one uses the cascade decay $\bar B^0\to D^{*+}(\to D^0\pi^+)\ell^-\bar\nu_\ell$ to analyze the polarization of the D^* meson. The derivation of the four-fold angular decay distribution is detailed in the Appendix. One has

$$\frac{d\Gamma(\bar B^0\to D^{*+}(\to D^0\pi^+)\ell^-\bar\nu_\ell)}{dq^2 d\cos\theta d(\chi/2\pi)d\cos\theta^*} = \frac{G_F^2}{(2\pi)^3}\frac{|V_{cb}|^2|\mathbf{p_2}|q^2v^2}{12m_1^2}\mathrm{Br}(D^*\to D\pi)W(\theta^*,\theta,\chi), \quad (55)$$

where

$$W(\theta^*,\theta,\chi) = \frac{9}{32}(1+\cos^2\theta)\sin^2\theta^*\mathcal{H}_U + \frac{9}{8}\sin^2\theta\cos^2\theta^*\mathcal{H}_L - \frac{9}{16}\cos\theta\sin^2\theta^*\mathcal{H}_P - \frac{9}{16}\sin^2\theta\sin^2\theta^*\cos 2\chi\mathcal{H}_T$$
$$- \frac{9}{8}\sin\theta\sin 2\theta^*\cos\chi\mathcal{H}_A + \frac{9}{16}\sin 2\theta\sin 2\theta^*\cos\chi\mathcal{H}_I + \frac{9}{8}\sin\theta\sin 2\theta^*\sin\chi\mathcal{H}_{II} - \frac{9}{16}\sin 2\theta\sin 2\theta^*\sin\chi\mathcal{H}_{IA}$$
$$+ \frac{9}{16}\sin^2\theta\sin^2\theta^*\sin 2\chi\mathcal{H}_{IT} + \delta_\ell\left[\frac{9}{4}\cos^2\theta^*\mathcal{H}_S - \frac{9}{2}\cos\theta\cos^2\theta^*\mathcal{H}_{SL} + \frac{9}{4}\cos^2\theta\cos^2\theta^*\mathcal{H}_L + \frac{9}{16}\sin^2\theta\sin^2\theta^*\mathcal{H}_U\right.$$
$$+ \frac{9}{8}\sin^2\theta\sin^2\theta^*\cos 2\chi\mathcal{H}_T + \frac{9}{4}\sin\theta\sin 2\theta^*\cos\chi\mathcal{H}_{ST} - \frac{9}{8}\sin 2\theta\sin 2\theta^*\cos\chi\mathcal{H}_I - \frac{9}{4}\sin\theta\sin 2\theta^*\sin\chi\mathcal{H}_{ISA}$$
$$\left. + \frac{9}{8}\sin 2\theta\sin 2\theta^*\sin\chi\mathcal{H}_{IA} - \frac{9}{8}\sin^2\theta\sin^2\theta^*\sin 2\chi\mathcal{H}_{IT}\right]. \quad (56)$$

In our quark model all helicity amplitudes are real, which implies the vanishing of all terms proportional to $\sin\chi$ and $\sin 2\chi$. The angular decay distribution for the remaining terms agrees with the results of Refs. [59–61] when one takes into account the different definition of the polar angle θ used in Refs. [59–61] such that $\theta \to 180^\circ - \theta$.

The four-fold distribution allows one to define a number of physical observables which can be measured experimentally. By integrating Eq. (56) over $\cos\theta^*$ and χ, one recovers the two-fold (q^2, $\cos\theta$) distribution of Eq. (46) that gives rise to the lepton-side forward-backward asymmetry parameter A_{FB} and the convexity parameter $C_F^\ell(q^2)$. By integrating Eq. (56) over $\cos\theta$ and χ, one obtains the hadron-side $\cos\theta^*$ distribution described by an untilted parabola (without a linear term). The normalized form of the $\cos\theta^*$ distribution reads $\tilde{W}(\theta^*) = (a' + c'\cos^2\theta^*)/2(a' + c'/3)$, which can again be characterized by its convexity parameter, given by

$$C_F^h(q^2) = \frac{d^2\widetilde{W}(\theta)}{d(\cos\theta^*)^2} = \frac{c'}{a' + c'/3}$$
$$= -\frac{3}{2}\frac{\mathcal{H}_U - 2\mathcal{H}_L + \delta_\ell(\mathcal{H}_U - 2\mathcal{H}_L - 6\mathcal{H}_S)}{\mathcal{H}_{\rm tot}}. \quad (57)$$

We define a normalized angular decay distribution $\tilde{W}(\theta^*,\theta,\chi)$ through

$$\tilde{W}(\theta^*,\theta,\chi) = \frac{W(\theta^*,\theta,\chi)}{\mathcal{H}_{\rm tot}}. \quad (58)$$

The normalized angular decay distribution $\tilde{W}(\theta^*,\theta,\chi)$ obviously integrates to 1 after $\cos\theta^*$, $\cos\theta$, and $\chi/2\pi$ integration.

The remaining coefficient functions $\mathcal{H}_T(1-2\delta_\ell)$, $\mathcal{H}_T(1-2\delta_\ell)$, and $(\mathcal{H}_A - 2\delta_\ell\mathcal{H}_{ST})$ in Eq. (56) can be projected from the three-fold angular decay distribution of Eq. (56) by taking the appropriate trigonometric moments of the normalized decay distribution $\tilde{W}(\theta^*,\theta,\chi)$. The trigonometric moments are defined by

$$W_i = \int d\cos\theta d\cos\theta^* d(\chi/2\pi) M_i(\theta^*,\theta,\chi)\widetilde{W}(\theta^*,\theta,\chi)$$
$$\equiv \langle M_i(\theta^*,\theta,\chi)\rangle, \quad (59)$$

where $M_i(\theta^*,\theta,\chi)$ defines the trigonometric moment that is being taken. One finds

$$W_T(q^2) \equiv \langle\cos 2\chi\rangle = -\frac{1}{2}(1-2\delta_\ell)\frac{\mathcal{H}_T}{\mathcal{H}_{\rm tot}},$$
$$W_I(q^2) \equiv \langle\cos\theta\cos\theta^*\cos\chi\rangle = \frac{9\pi^2(1-2\delta_\ell)}{512}\frac{\mathcal{H}_I}{\mathcal{H}_{\rm tot}},$$
$$W_A(q^2) \equiv \langle\sin\theta\cos\theta^*\cos\chi\rangle = -\frac{3\pi}{16}\frac{\mathcal{H}_A - 2\delta_\ell\mathcal{H}_{ST}}{\mathcal{H}_{\rm tot}}. \quad (60)$$

The coefficient functions $\mathcal{H}_T(1-2\delta_\ell)$, $\mathcal{H}_T(1-2\delta_\ell)$, and $(\mathcal{H}_A - 2\delta_\ell\mathcal{H}_{ST})$ can also be projected out by taking piecewise sums and differences of different sectors of the angular phase space [60].

Finally, we consider the longitudinal and transverse polarizations of the lepton, where we consider only the angular average of the two polarization states. For the longitudinal polarization one obtains

$$P_z^\ell(q^2) = \frac{\delta_\ell\mathcal{H}_{hf} - \mathcal{H}_{nf}}{\delta_\ell\mathcal{H}_{hf} + \mathcal{H}_{nf}}$$
$$= -\frac{\mathcal{H}_U + \mathcal{H}_L - \delta_\ell(\mathcal{H}_U + \mathcal{H}_L + 3\mathcal{H}_S)}{\mathcal{H}_{\rm tot}}. \quad (61)$$

The transverse polarization can be calculated using the representation of the polarized lepton tensor written down in the appendix of Ref. [40]. One obtains

$$P_x^\ell(q^2) = -\frac{3\pi\sqrt{\delta_\ell}}{4\sqrt{2}}\frac{\mathcal{H}_P - 2\mathcal{H}_{SL}}{\mathcal{H}_{\rm tot}}. \quad (62)$$

For the decay $B \to D\ell^-\bar{\nu}_\ell$, one has to drop the transverse contributions $\mathcal{H}_U$ and $\mathcal{H}_P$ in Eqs. (61) and (62). It is interesting to note that for this decay there exists a very

simple relation connecting $P_x^\ell(q^2)$ and $A_{FB}(q^2)$ which reads

$$P_x^\ell(q^2) = -\frac{\pi\sqrt{q^2}}{2m_\tau} A_{FB}(q^2). \tag{63}$$

The polarization of the lepton depends on the frame in which it is defined. The polarization components P_z^ℓ and P_x^ℓ in (61) and (62) are calculated in the $(\ell^-\bar{\nu}_\tau)$ rest frame. The corresponding polarization components in the B rest frame have been calculated in Ref. [62].

VIII. RESULTS AND DISCUSSION

The values of the lepton and meson masses and their lifetimes are taken from Ref. [45]. We also adopt the following values for the CKM matrix elements: $|V_{ub}| = 0.00413$ and $|V_{bc}| = 0.0411$. In Fig. 7 we represent our results for the differential branching fractions of the decays $B \to D^{(*)}\ell\nu$ within the full range of the momentum transfer squared. For comparison, we also display the form factors calculated in the heavy quark limit. It is readily seen that the two forms are very close to each other. It confirms that HQET works very well in the leading order for b-c transitions. In what follows, we will not display the curves for observables obtained in the HQL.

In Fig. 8 we represent our results for the forward-backward asymmetries of the decays $B \to D^{(*)}\ell\nu$ within the full range of the momentum transfer squared. The forward-backward asymmetry for the decay $B \to D\tau^-\bar{\nu}_\tau$ is quite large in the lower half of the q^2 spectrum, which can be understood from the fact that $A_{FB} = -3\delta_\ell \mathcal{H}_{SL}$ and that $3\delta(q^2)$ is large in the threshold region. It is quite interesting that the forward-backward asymmetry for the decay $B \to D^*\tau^-\bar{\nu}_\tau$ goes through zero at $q^2 = 6.25\ \mathrm{GeV}^2$.

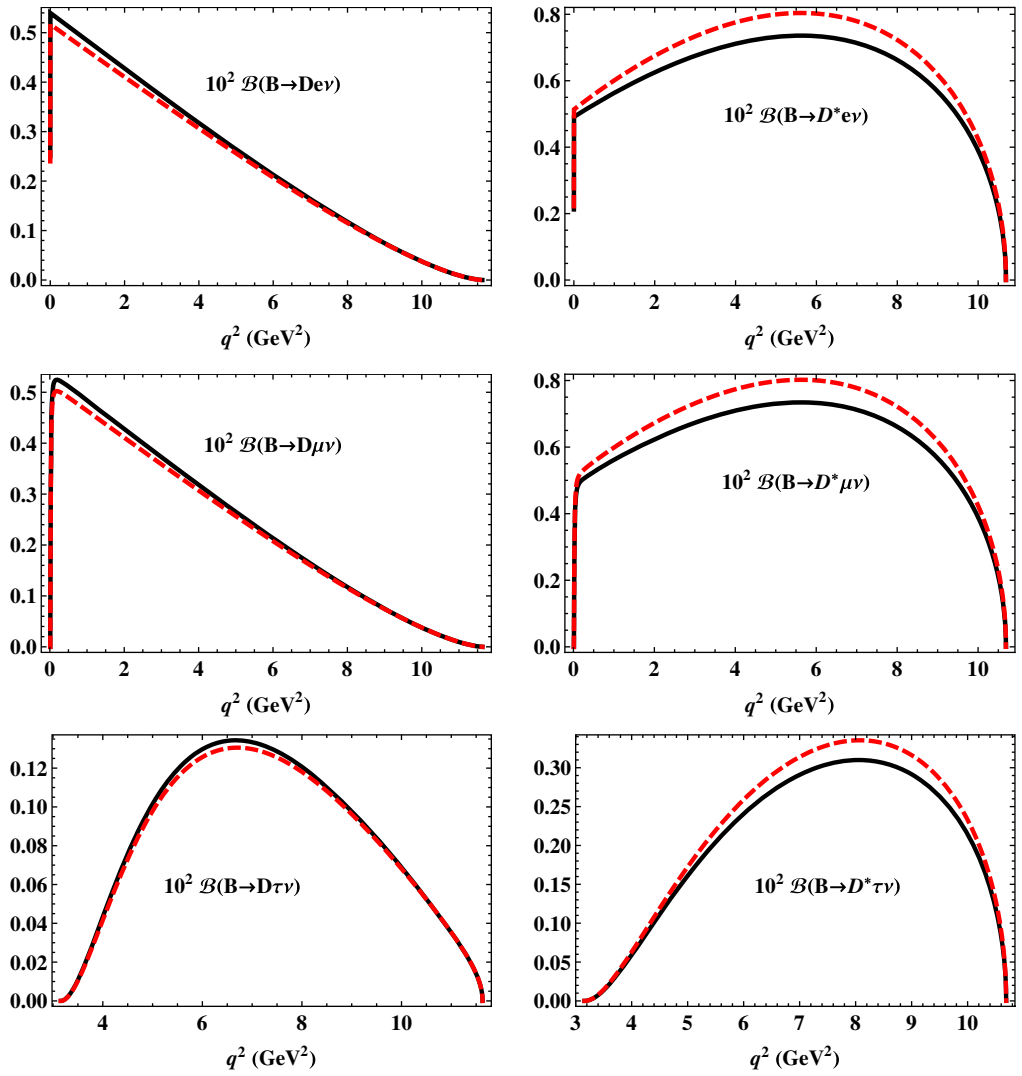

FIG. 7 (color online). Differential branching fractions of the decays $B \to D^{(*)}\ell\nu$. The solid lines are the results of exact calculations in our approach; the dashed lines are the form factors obtained in the heavy quark limit.

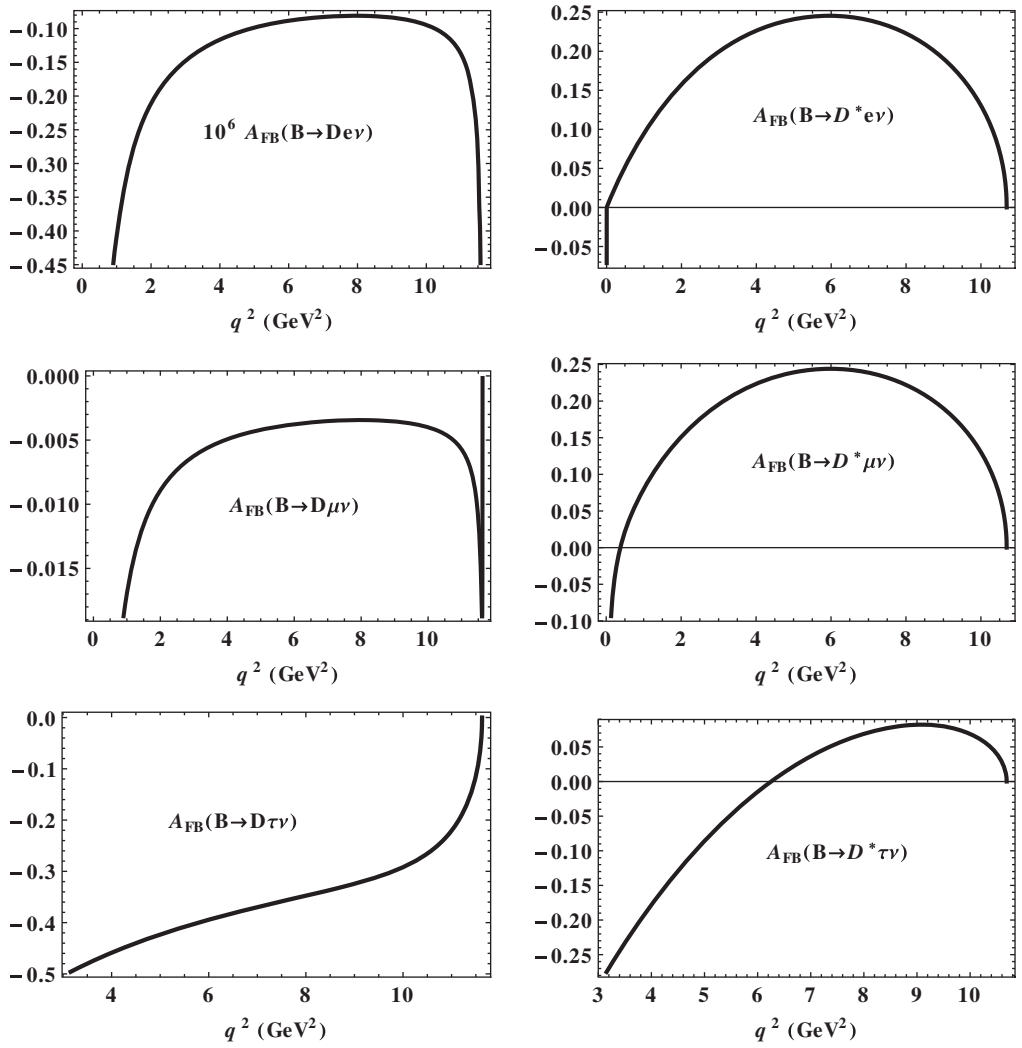

FIG. 8. Forward-backward asymmetries of the decays $B \to D^{(*)}\ell\nu$.

TABLE II. Definition of helicity structure functions and their parity properties for the case $B \to D^*\ell^-\bar{\nu}_\ell$.

Parity-conserving (p.c.)	Parity-violating (p.v.)
$\mathcal{H}_U = \lvert H_{+1+1}\rvert^2 + \lvert H_{-1-1}\rvert^2$	$\mathcal{H}_P = \lvert H_{+1+1}\rvert^2 - \lvert H_{-1-1}\rvert^2$
$\mathcal{H}_L = \lvert H_{00}\rvert^2$	$\mathcal{H}_A = \frac{1}{2}\mathrm{Re}(H_{+1+1}H_{00}^\dagger - H_{-1-1}H_{00}^\dagger)$
$\mathcal{H}_T = \mathrm{Re}(H_{+1+1}H_{-1-1}^\dagger)$	$\mathcal{H}_{IA} = \frac{1}{2}\mathrm{Im}(H_{+1+1}H_{00}^\dagger - H_{-1-1}H_{00}^\dagger)$
$\mathcal{H}_{IT} = \mathrm{Im}(H_{+1+1}H_{-1-1}^\dagger)$	$\mathcal{H}_{SA} = \frac{1}{2}\mathrm{Re}(H_{+1+1}H_{0t}^\dagger - H_{-1-1}H_{0t}^\dagger)$
$\mathcal{H}_I = \frac{1}{2}\mathrm{Re}(H_{+1+1}H_{00}^\dagger + H_{-1-1}H_{00}^\dagger)$	$\mathcal{H}_{ISA} = \frac{1}{2}\mathrm{Im}(H_{+1+1}H_{0t}^\dagger - H_{-1-1}H_{0t}^\dagger)$
$\mathcal{H}_{II} = \frac{1}{2}\mathrm{Im}(H_{+1+1}H_{00}^\dagger + H_{-1-1}H_{00}^\dagger)$	
$\mathcal{H}_S = \lvert H_{0t}\rvert^2$	
$\mathcal{H}_{ST} = \frac{1}{2}\mathrm{Re}(H_{+1+1}H_{0t}^\dagger + H_{-1-1}H_{0t}^\dagger)$	
$\mathcal{H}_{IST} = \frac{1}{2}\mathrm{Im}(H_{+1+1}H_{0t}^\dagger + H_{-1-1}H_{0t}^\dagger)$	
$\mathcal{H}_{SL} = \mathrm{Re}(H_{00}H_{0t}^\dagger)$	
$\mathcal{H}_{ISL} = \mathrm{Im}(H_{00}H_{0t}^\dagger)$	
$\mathcal{H}_{\mathrm{tot}} = \mathcal{H}_U + \mathcal{H}_L + \delta_\ell(\mathcal{H}_U + \mathcal{H}_L + 3\mathcal{H}_S)$	

TABLE III. Leptonic B-decay branching fractions.

	This work	Data	Reference
$B^- \to e^- \bar{\nu}_e$	1.16×10^{-11}	$<9.8 \times 10^{-7}$	PGD [45]
		$(0.88 \pm 0.12) \times 10^{-11}$	UTfit [4]
		$(0.85 \pm 0.27) \times 10^{-11}$	CKMfitter [63]
$B^- \to \mu^- \bar{\nu}_\mu$	0.49×10^{-6}	$<1.0 \times 10^{-6}$	PGD [45]
		$(0.38 \pm 0.05) \times 10^{-6}$	UTfit [4]
		$(0.37 \pm 0.02) \times 10^{-6}$	CKMfitter [63]
$B^- \to \tau^- \bar{\nu}_\tau$	1.10×10^{-4}	$(1.14 \pm 0.27) \times 10^{-4}$	PGD [45]

The branching fractions of the decays $B \to \ell^- \bar{\nu}$, $B \to D^{(*)} \ell^- \bar{\nu}$, and $B \to \pi \ell^- \bar{\nu}$, as well as the ratios of branching fractions $R(D^{(*)})$ are presented in Tables III, IV, and V. The branching fractions $\mathcal{B}(B \to \ell^- \bar{\nu})$, $(\ell = e, \mu)$ satisfy the experimental constraints and show good agreement with the CKMfitter results, while the branching fraction $\mathcal{B}(B \to \tau^- \bar{\nu}_\tau)$ is consistent with experimental data, giving more constraints on NP effects that may contribute to the transitions. The situation is different for the semileptonic decays. The results for $\mathcal{B}(B \to D^{(*)} \ell^- \bar{\nu})$ are slightly larger, while the results for $\mathcal{B}(B \to D^{(*)} \tau^- \bar{\nu}_\tau)$ are slightly smaller in comparison with experimental data. As a result, the calculated ratios $R(D^{(*)})$ are slightly smaller than the SM expectation, which means they deviate from the experimental values even more. This may imply the appearance of NP.

TABLE IV. Semileptonic decay branching fractions of B mesons. The values obtained in the HQL are given in brackets. The experimental errors are combined in quadrature.

	Unit	This work	Data	Reference
$\bar{B}^0 \to D^+ \ell^- \bar{\nu}$	10^{-2}	2.74(2.65)	2.17 ± 0.12	HFAG [9]
			2.21 ± 0.16	*BABAR* [64]
$\bar{B}^0 \to D^+ \tau^- \bar{\nu}_\tau$	10^{-2}	0.73(0.71)	1.02 ± 0.17	*BABAR* [10]
$\bar{B}^0 \to D^{*+} \ell^- \bar{\nu}$	10^{-2}	6.64(7.21)	5.05 ± 0.12	HFAG [9]
			5.49 ± 0.30	*BABAR* [64]
$\bar{B}^0 \to D^{*+} \tau^- \bar{\nu}_\tau$	10^{-2}	1.57(1.70)	1.76 ± 0.18	*BABAR* [10]
$\bar{B}^0 \to \pi^+ \ell^- \bar{\nu}$	10^{-4}	1.69	1.41 ± 0.09	*BABAR* [7]
			1.49 ± 0.08	Belle [8]
$\bar{B}^0 \to \pi^+ \tau^- \bar{\nu}_\tau$	10^{-4}	1.01	…	…

TABLE V. Ratios of branching fractions $R(D)$ and $R(D^*)$ calculated in our model (the values obtained in the HQL are given in brackets) and compared with the SM expectations and experimental data.

	This work	SM	Data
$R(D)$	0.265(0.268)	0.297 ± 0.017	0.388 ± 0.047
$R(D^*)$	0.237(0.235)	0.252 ± 0.003	0.321 ± 0.021

Next, we define the partial helicity rates by

$$\frac{d\Gamma_X}{dq^2} = \frac{G_F^2}{(2\pi)^3} \frac{|V_{cb}|^2 |\mathbf{p_2}| q^2 v^2}{12 m_1^2} \mathcal{H}_X,$$
$$\frac{d\tilde{\Gamma}_X}{dq^2} = \delta_\ell \frac{d\Gamma_X}{dq^2}, \tag{64}$$

where $X = U, L, P, \ldots$. In Figs. 9 and 10 we display the q^2 dependence of the partial differential rates $d\Gamma_U/dq^2$, $d\Gamma_L/dq^2$, and the total differential rate $d\Gamma_{U+L}/dq^2$ for the e mode. The transverse rate dominates in the low-recoil region, while the longitudinal rate dominates in the large-recoil region. The longitudinal, and thereby the total, rate shows a steplike behavior near the threshold $q^2 = m_e^2$. Figures 11 and 12 show the corresponding plots for the τ mode, including the partial flip rates $d\tilde{\Gamma}_{U,L}/dq^2$ and $3d\tilde{\Gamma}_S/dq^2$. We also show the total differential rate $d\Gamma_{U+L}/dq^2 + d\tilde{\Gamma}_{U+L+3S}/dq^2$. The helicity flip rates are smaller than the helicity nonflip rates but contribute significantly to the total rate.

In Figs. 13, 14, and 15 we display the q^2 dependence of the convexity parameters C_F^ℓ and C_F^h for the lepton and hadron sides defined in Eqs. (52) and (57). In the $B \to D$ case, the $\cos\theta$ distribution is described by a downward open parabola which becomes much flatter for the τ mode. We do not plot the hadron-side convexity parameter $C_F^h(q^2)$ for the $B \to D$ transition, since it trivially reads $C_F^h = 3$ following from the definition (57). For the $B \to D^*$ transition, the lepton-side $\cos\theta$ distribution is again described by a downward open parabola which becomes almost flat for the τ mode. The hadron-side $\cos\theta^*$ distribution is described by an upward open parabola which does not become flat at the zero-recoil point. Lepton mass effects are not very pronounced.

In Figs. 16, 17, and 18 we show plots of the q^2 dependence of the longitudinal, transverse, and total polarization of the lepton for the $B \to D \ell^- \bar{\nu}_\ell$ transition. In the case of the electron, the curves reflect the chiral limit

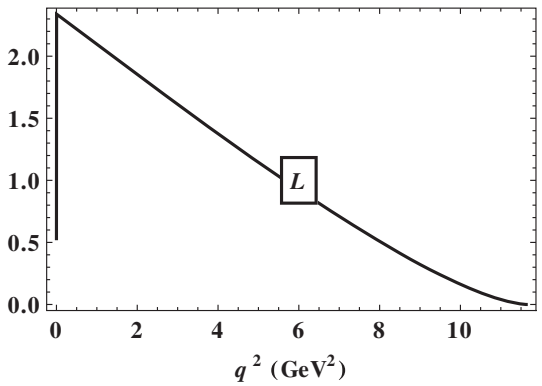

FIG. 9. *$B \to D$ transition*: The q^2 dependence of the partial rate $d\Gamma_L/dq^2$ for the e^- mode (in units of 10^{-15} GeV^{-1}).

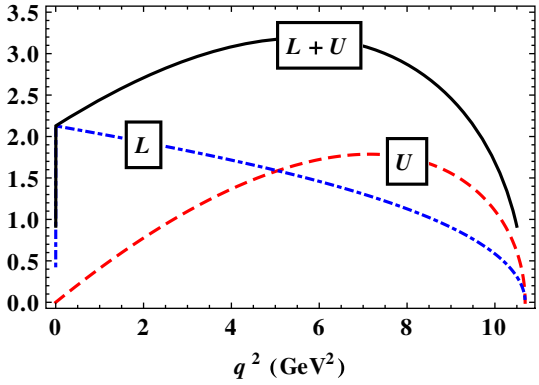

FIG. 10 (color online). $B \to D^*$ *transition*: The q^2 dependence of the partial rates $d\Gamma_U/dq^2$ (dashed), $d\Gamma_L/dq^2$ (dot-dashed) and their sum $d\Gamma_{U+L}/dq^2$ (solid) for the e^- mode (in units of 10^{-15} GeV^{-1}).

of a massless lepton in which the lepton is purely left-handed, i.e. one has $P_z^\ell = -1$, $P_x^\ell = 0$, and $|\vec{P}^\ell| = 1$. For $\ell = \tau$ the transverse polarization is large and positive and dominates the total polarization. The transverse polarization of the τ drops out after the appropriate azimuthal averaging, as has been done in Ref. [13]. Note that the transverse polarization in the τ mode results solely from the scalar-longitudinal interference contribution $\mathcal{H}_{SL}$. The longitudinal polarization has switched its sign relative to the $m_\ell = 0$ case.

The corresponding curves for the $B \to D^* \ell^- \bar{\nu}_\ell$ transition are shown in Figs. 19,20, and 21. The longitudinal and transverse polarization components are distinctly different from their $m_\ell = 0$ values $P_z^\ell = -1$ and $P_x^\ell = 0$. The longitudinal component becomes larger in magnitude when q^2 increases, while the transverse polarization becomes smaller as q^2 increases. At zero recoil, the transverse polarization of the charged lepton P_x^τ tends to zero in agreement with the vanishing of $\mathcal{H}_P$ and $\mathcal{H}_{SL}$ at zero recoil. The total polarization of the τ shown in Fig. 21 has an almost flat behavior with $|\vec{P}^\ell| \sim 0.7$. The overall picture is that the polarization is mostly transverse at threshold and turns to longitudinal as q^2 reaches the zero-recoil point.

In Figs. 22,23, and 24 we display the q^2 dependence of the three trigonometric moments $W_i (i = T, I, A)$ of the normalized three-fold angular function $\tilde{W}(\theta^*, \theta, \chi)$ defined in Eq. (60). Lepton mass effects can be seen to be quite large for all three moments.

Finally, in Figs. 25 and 26 we present the q^2 dependence of the rate ratios ($\ell = e, \mu$)

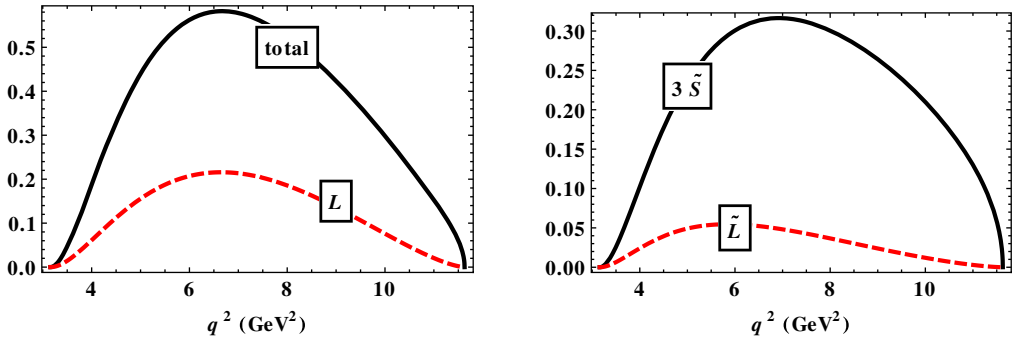

FIG. 11 (color online). $B \to D$ *transition*: The q^2 dependence of the partial nonflip rates $d\Gamma_L/dq^2$, and the flip rates $d\tilde{\Gamma}_{U,L}/dq^2$ and $3d\tilde{\Gamma}_S/dq^2$ for the τ^- mode (in units of 10^{-15} GeV^{-1}). Also shown is the total rate $d\Gamma_L/dq^2 + d\tilde{\Gamma}_L/dq^2 + 3d\tilde{\Gamma}_S/dq^2$.

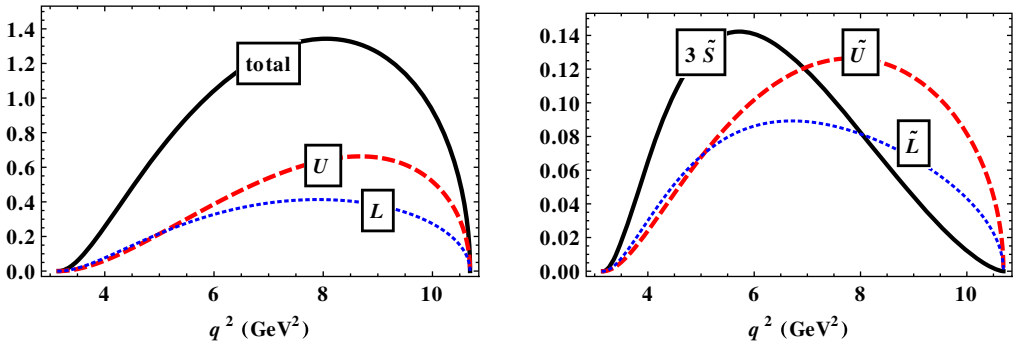

FIG. 12 (color online). $B \to D^*$ *transition*: The q^2 dependence of the partial nonflip rates $d\Gamma_{U,L}/dq^2$, and the flip rates $d\tilde{\Gamma}_{U,L}/dq^2$ and $3d\tilde{\Gamma}_S/dq^2$ for the τ^- mode (in units of 10^{-15} GeV^{-1}). Also shown is the total rate $d\Gamma_{U+L}/dq^2 + d\tilde{\Gamma}_{U+L}/dq^2 + 3d\tilde{\Gamma}_S/dq^2$.

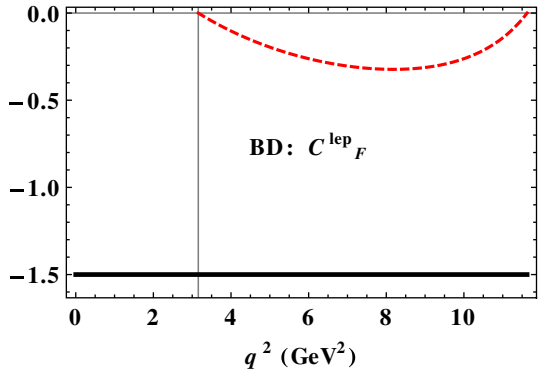

FIG. 13 (color online). $B \to D$ *transition*: The q^2 dependence of the lepton convexity parameter $C_F^{\ell}(q^2)$ for the e^--mode (solid) and τ^--mode (dashed).

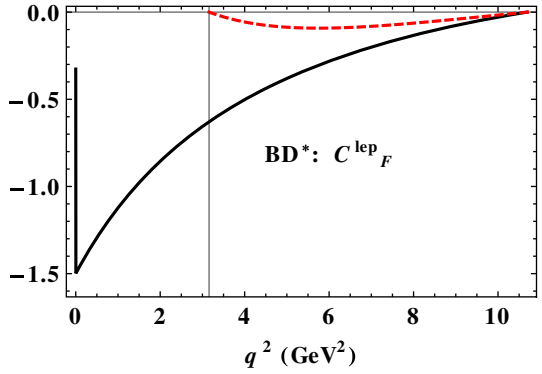

FIG. 14 (color online). $B \to D^*$ *transition*: The q^2 dependence of the lepton convexity parameter $C_F^{\ell}(q^2)$ for the e^--mode (solid) and τ^--mode (dashed).

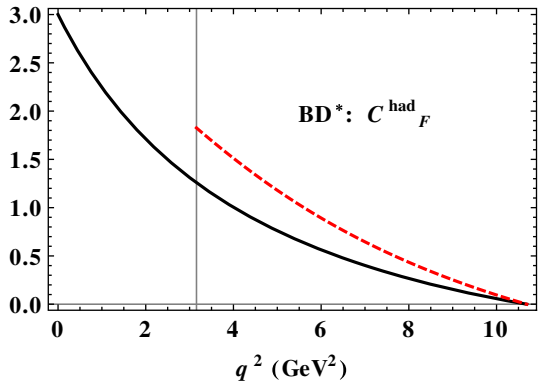

FIG. 15 (color online). $B \to D^*$ *transition*: The q^2 dependence of the hadron convexity parameter $C_F^{h}(q^2)$ for the e^--mode (solid) and τ^--mode (dashed).

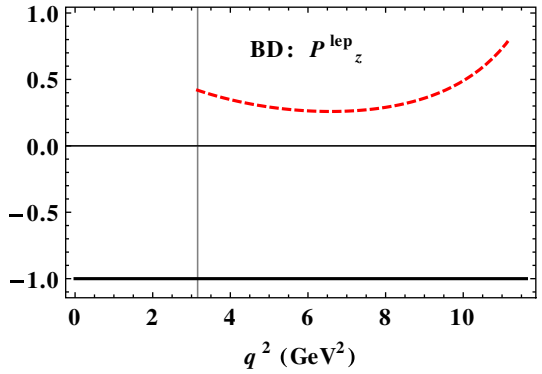

FIG. 16 (color online). $B \to D$ *transition*: The q^2 dependence of the longitudinal polarization component $P_z^{\ell}(q^2)$ for the charged leptons e^--mode (solid) and τ^--mode (dashed).

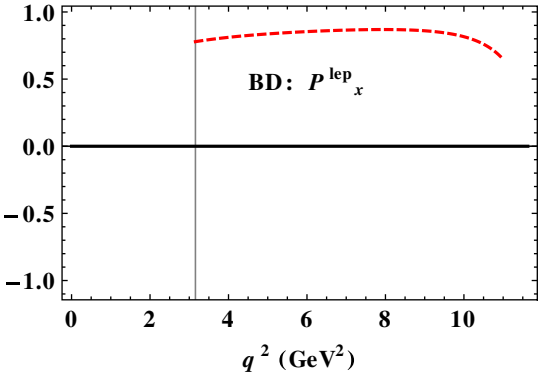

FIG. 17 (color online). $B \to D$ *transition*: The q^2 dependence of the transverse polarization component $P_x^{\ell}(q^2)$ for the charged leptons e^--mode (solid) and τ^--mode (dashed).

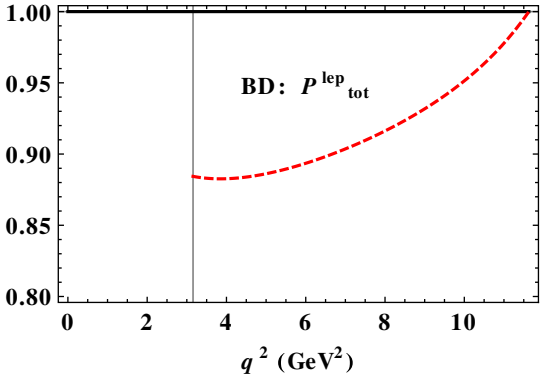

FIG. 18 (color online). $B \to D$ *transition*: The q^2 dependence of the total lepton polarization $|\vec{P}^{\ell}|(q^2) = \sqrt{(P_x^{\ell})^2 + (P_z^{\ell})^2}$ for the e^--mode (solid) and τ^--mode (dashed).

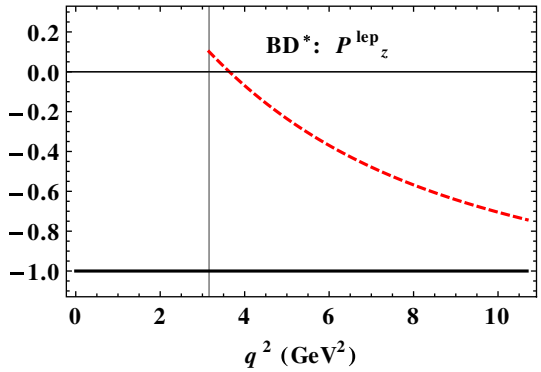

FIG. 19 (color online). $B \to D^*$ *transition*: The q^2 dependence of the longitudinal polarization component $P_z^{\ell}(q^2)$ for the charged leptons e^--mode (solid) and τ^--mode (dashed).

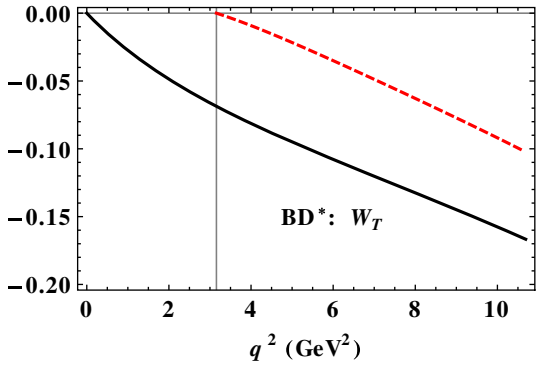

FIG. 22 (color online). $B \to D^*$ *transition*: The q^2 dependence of the trigonometric moment W_T defined in Eq. (60) for the e^--mode (solid) and τ^--mode (dashed).

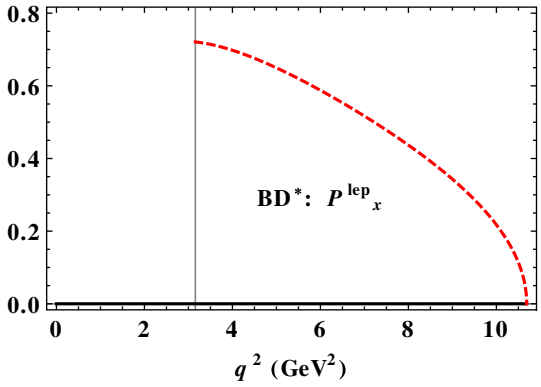

FIG. 20 (color online). $B \to D^*$ *transition*: The q^2 dependence of the transverse polarization component $P_x^{\ell}(q^2)$ for the charged leptons e^--mode (solid) and τ^--mode (dashed).

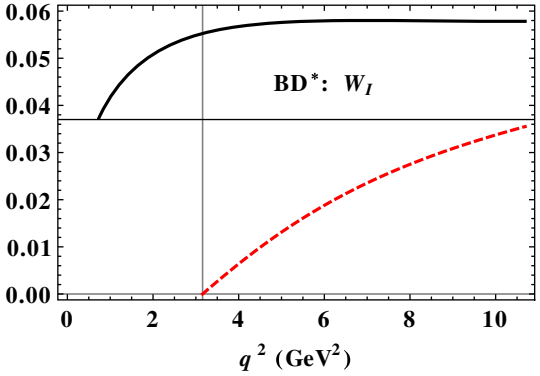

FIG. 23 (color online). $B \to D^*$ *transition*: The q^2 dependence of the trigonometric moment W_I defined in Eq. (60) for the e^--mode (solid) and τ^--mode (dashed).

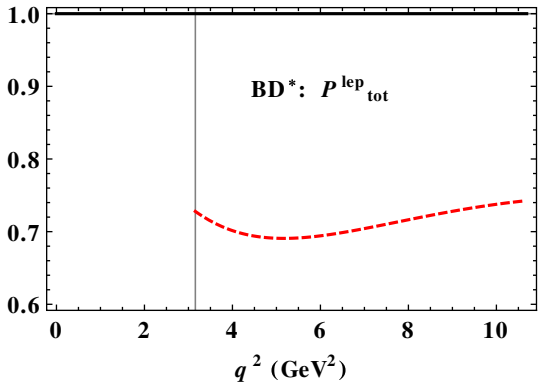

FIG. 21 (color online). $B \to D^*$ *transition*: The q^2 dependence of the total lepton polarization $|\vec{P}^{\ell}|(q^2) = \sqrt{(P_x^{\ell})^2 + (P_z^{\ell})^2}$ for the e^--mode (solid) and τ^--mode (dashed).

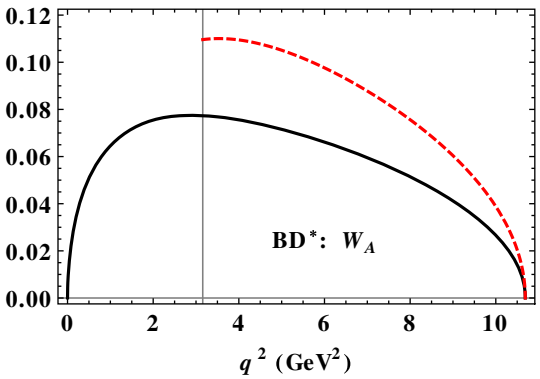

FIG. 24 (color online). $B \to D^*$ *transition*: The q^2 dependence of the trigonometric moment W_A defined in Eq. (60) for the e^--mode (solid) and τ^--mode (dashed).

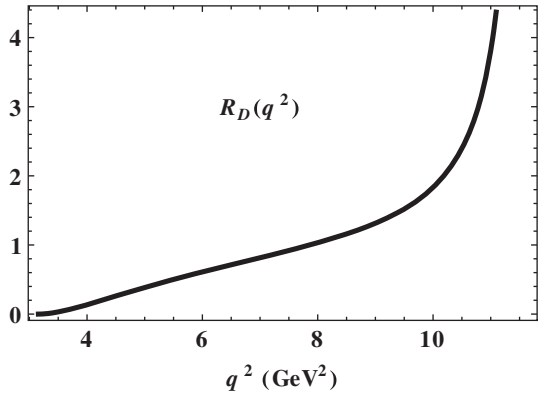

FIG. 25. The q^2 dependence of the ratio $R(D)$.

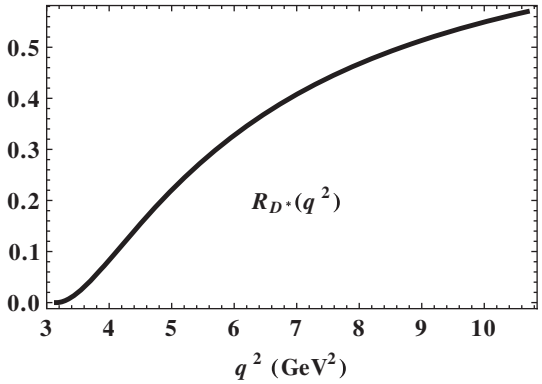

FIG. 26. The q^2 dependence of the ratio $R(D^*)$.

$$R_{D^{(*)}}(q^2) = \frac{d\Gamma(B \to D^{(*)}\tau^-\bar{\nu}_\tau)}{dq^2} \Big/ \frac{d\Gamma(B \to D^{(*)}\ell^-\bar{\nu}_\ell)}{dq^2}. \tag{65}$$

Hopefully there will be enough data in the future to explore the apparent flavor violation in the tauonic semileptonic $B \to D^{(*)}$ transitions in more detail by measuring the rate ratios in different q^2 bins.

TABLE VI. q^2 averages of the rate functions in units of 10^{-15} GeV. We do not display the helicity flip results for the e mode, because they are of the order of 10^{-6}–10^{-7} in the above units.

$B \to D$							
	Γ_L						
e	11.9						
τ	1.05						
	$\tilde{\Gamma}_L$	$\tilde{\Gamma}_S$	$\tilde{\Gamma}_{SL}$				
τ	0.25	0.62	0.38				
$B \to D^*$							
	Γ_U	Γ_L	Γ_T	Γ_I	Γ_P	Γ_A	
e	13.2	15.6	5.35	8.94	−7.42	−3.01	
τ	3.02	2.08	1.32	1.70	−1.42	−0.44	
	$\tilde{\Gamma}_U$	$\tilde{\Gamma}_L$	$\tilde{\Gamma}_T$	$\tilde{\Gamma}_I$	$\tilde{\Gamma}_S$	$\tilde{\Gamma}_{SL}$	$\tilde{\Gamma}_{ST}$
τ	0.64	0.46	0.27	0.37	0.20	0.29	0.22

TABLE VII. q^2 averages of polarization observables. For comparison with results from the HQL, we add in brackets the corresponding HQL values.

$B \to D$			
	$\langle A_{FB}^\ell \rangle$	$\langle C_F^\ell \rangle$	$\langle C_F^h \rangle$
e	$-1.17(-1.16) \times 10^{-6}$	−1.5(−1.5)	3(3)
τ	−0.36(−0.36)	−0.26(−0.26)	3(3)
	$\langle P_z^\ell \rangle$	$\langle P_x^\ell \rangle$	$\langle \lvert\vec{P}^\ell\rvert \rangle$
e	−1(−1)	0(0)	1(1)
τ	0.33(0.33)	0.84(0.84)	0.91(0.91)
$B \to D^*$			
	$\langle A_{FB}^\ell \rangle$	$\langle C_F^\ell \rangle$	$\langle C_F^h \rangle$
e	0.19(0.18)	−0.47(−0.44)	0.93(0.88)
τ	0.027(0.021)	−0.062(−0.057)	0.58(0.52)
	$\langle P_z^\ell \rangle$	$\langle P_x^\ell \rangle$	$\langle \lvert\vec{P}^\ell\rvert \rangle$
e	−1(−1)	0(0)	1(1)
τ	−0.50(−0.51)	0.46(0.43)	0.71(0.71)
	$\langle W_T \rangle$	$\langle W_I \rangle$	$\langle W_A \rangle$
e	−0.093(−0.098)	0.054(0.055)	0.062(0.059)
τ	−0.057(−0.059)	0.025(0.025)	0.077(0.074)

Next, we present our model results for the average values of the rate functions in Table VI. And in Table VII we show the average values of the polarization observables: the forward-backward asymmetry $\langle A_{FB} \rangle$, the convexity parameter $\langle C_F \rangle$, the leptonic $\langle P_{x,z}^\ell \rangle$ polarization components, and the three trigonometric moments $< W_i (i = T, I, A)$. Lepton mass effects can be seen to be quite large for the average values of the polarization observables.

IX. SUMMARY AND CONCLUSIONS

We have provided a detailed analysis of the pure leptonic and semileptonic decays $B \to \ell^-\bar{\nu}_\ell$ and $B \to D^{(*)}\ell^-\bar{\nu}_\ell$ ($\ell = e, \mu, \tau$) within the SM in the framework of our covariant quark model with built-in quark confinement. We have described in some detail how to compute the one-loop quark contributions needed for the calculation of the transition form factors, including a discussion of how the confinement of the constituent quarks is achieved in the covariant quark model. In the light of the recent experimental indications for a possible breaking of lepton universality in the τ sector, we have put particular emphasis on how to isolate heavy lepton mass effects in the semileptonic decays.

We have described how to obtain the full angular decay distributions for $B \to D\ell^-\bar{\nu}_\ell$ and the cascade decay process $B \to D^*(\to D\pi)\ell^-\bar{\nu}_\ell$, as well as the corresponding angular decay distributions for their charge-conjugate processes. The coefficients multiplying the angular factors in the angular decay distributions have been given in terms of helicity structure functions for which we have provided

simple expressions for the maximal recoil $q^2 = 0$ and the minimal (zero) recoil $q^2 = (m_1 - m_2)^2$. Starting from the angular decay distributions, we have defined a multitude of polarization observables, for which we have provided numerical results on their q^2 spectra and their q^2 averages for zero and nonzero lepton masses. The polarization observables include the transverse and longitudinal polarizations of the charged τ^- which considerably deviate from their simple $m_\ell = 0$ left-chiral structure.

We are looking forward to a wealth of data on these decays expected in the near future which will allow us to deeply probe into their decay structure, in particular for the tauonic mode. Such an analysis will reveal possible deviations from the SM predictions not only in the branching fractions of the processes but also in the multitude of polarization observables and their q^2 spectra.

ACKNOWLEDGMENTS

M. A. I. acknowledges the support from the Mainz Institute for Theoretical Physics (MITP). M. A. I. and J. G. K. thank the Heisenberg-Landau Grant for providing support for their collaboration.

APPENDIX: SPIN KINEMATICS

In this appendix we provide a synopsis of how to obtain the angular decay distributions for the decays $B \to D^{(*)}\ell^-\bar{\nu}_\ell$ following the description in Refs. [40,65]. The covariant representation of the angular decay distribution is given by

$$W'(\theta^*, \theta, \chi) = h_{\alpha'\beta'} P_1^{\alpha'\alpha} P_1^{\beta'\beta} H_{\alpha\mu} H^\dagger_{\beta\nu} P^{\mu\mu'}_{0\oplus 1} P^{\nu\nu'}_{0\oplus 1} L_{\mu'\nu'}, \quad \text{(A1)}$$

where $h_{\alpha'\beta'}$ is the hadronic decay tensor for the decay $D^* \to D + \pi$ (with $h^{\alpha\beta} = p_3^\alpha p_3^\beta/|\mathbf{p_3}|^2$), $H_{\alpha\mu} H^\dagger_{\beta\nu}$ is the tensor describing the decay $B \to D^* + W^-_{\text{off-shell}}$, and $L_{\mu'\nu'}$ is the lepton tensor describing the decay $W^-_{\text{off-shell}} \to \ell^- + \bar{\nu}_\ell$. The tensors are connected by the appropriate spin-1 and spin-$(0 \oplus 1)$ propagator projectors $P_1^{\mu\nu}(q) = -g^{\mu\nu} + q^\mu q^\nu/q^2$ and $P^{\mu\nu}_{0\oplus 1}(q)$ which, in the unitary gauge, read [66]

$$P^{\nu\beta}_{0\oplus 1}(q) = -g^{\nu\beta} + \frac{q^\nu q^\beta}{m_W^2} = \underbrace{\left(-g^{\nu\beta} + \frac{q^\nu q^\beta}{q^2}\right)}_{\text{spin 1}} - \underbrace{\frac{q^\nu q^\beta}{q^2}\left(1 - \frac{q^2}{m_W^2}\right)}_{\text{spin 0}}, \quad \text{(A2)}$$

$$= P_1^{\nu\beta}(q) - \left(1 - \frac{q^2}{m_W^2}\right) P_0^{\nu\beta}(q), \quad \text{(A3)}$$

where $P_0^{\mu\nu}(q) = q^\mu q^\nu/q^2$ is the spin-0 propagator. The factor $(1 - q^2/m_W^2)$ multiplying the spin-0 propagator in Eq. (A2) is usually set to 1 in low-energy applications, as in the decay $B \to D^*\ell^-\bar{\nu}_\ell$. For example, at the highest q^2 value at $q^2 = (m_B - m_{D^*})^2$, the correction amounts to a mere 0.17% and will therefore be dropped in the following.

In order to convert the covariant representation of the angular decay distribution Eq. (A1) to the helicity representation, one makes use of the completeness relations

$$P^{\mu\nu}_{0\oplus 1}(q) = -g^{\mu\nu} + \frac{q^\nu q^\beta}{m_W^2} = -\sum_{m,m'=t,\pm,0} \varepsilon^\mu(m)\varepsilon^{\dagger\nu}(m') g_{mm'}, \quad \text{(A4)}$$

$$P_1^{\mu\nu}(q) = -g^{\mu\nu} + q^\mu q^\nu/q^2 = \sum_{m,m'=\pm,0} \varepsilon^\mu(m)\varepsilon^{\dagger\nu}(m'), \quad \text{(A5)}$$

where the tensor $g_{mm'} = \text{diag}(+,-,-,-)$ is the spherical representation of the metric tensor whose components are ordered in the sequence $m, m' = t, +, 0, -$. With the help of the completeness relation (A5), one can convert the covariant form of the angular decay distribution Eq. (A1) into the helicity form

$$W'(\theta^*, \theta, \chi) = \sum_{J,J',\lambda_W,\lambda'_W,\lambda_2,\lambda'_2} (-1)^{J+J'} \delta_{\lambda_2\lambda_W} \delta_{\lambda'_2\lambda'_W} h_{\lambda_2\lambda'_2}(\theta^*) \times H_{\lambda_2\lambda_W}(J) H^*_{\lambda'_2\lambda'_W}(J') L_{\lambda_W\lambda'_W}(J, J', \theta, \chi). \quad \text{(A6)}$$

In (A6) we have chosen a representation of the helicity amplitudes which is particularly well suited for computer processing. Compared to the helicity amplitudes introduced in the main text, we have used $H_{0\lambda_W=0}(J=0) \equiv H_{0t}$ and $H_{0,\pm 1\lambda_W=0,\pm}(J=1) \equiv H_{0,\pm 10,\pm 1}$.

The helicity representation of the hadronic decay tensor $h_{\alpha\beta}(\theta^*)$ describing the decay $D^* \to D\pi$ is given by

$$h_{\lambda_2\lambda'_2}(\theta^*) = d^1_{0\lambda_2}(\theta^*) d^1_{0\lambda'_2}(\theta^*) = \begin{pmatrix} \frac{1}{2}\sin^2\theta^* & \frac{1}{2\sqrt{2}}\sin 2\theta^* & -\frac{1}{2}\sin^2\theta^* \\ +\frac{1}{2\sqrt{2}}\sin 2\theta^* & \cos^2\theta^* & -\frac{1}{2\sqrt{2}}\sin 2\theta^* \\ -\frac{1}{2}\sin^2\theta^* & -\frac{1}{2\sqrt{2}}\sin 2\theta^* & \frac{1}{2}\sin^2\theta^* \end{pmatrix}. \quad \text{(A7)}$$

For the helicity representation of the lepton tensor, one obtains $(v = 1 - m_\ell^2/q^2)$ [40]

$$(2q^2v)^{-1}L_{\lambda_W\lambda'_W}(1,1,\theta,\chi) = \begin{pmatrix} (1\mp\cos\theta)^2 & \mp\frac{2}{\sqrt{2}}(1\mp\cos\theta)\sin\theta e^{i\chi} & \sin^2\theta e^{2i\chi} \\ \mp\frac{2}{\sqrt{2}}(1\mp\cos\theta)\sin\theta e^{-i\chi} & 2\sin^2\theta & \mp\frac{2}{\sqrt{2}}(1\pm\cos\theta)\sin\theta e^{i\chi} \\ \sin^2\theta e^{-2i\chi} & \mp\frac{2}{\sqrt{2}}(1\pm\cos\theta)\sin\theta e^{-i\chi} & (1\pm\cos\theta)^2 \end{pmatrix} + \delta_\ell \begin{pmatrix} 2\sin^2\theta & -\frac{2}{\sqrt{2}}\sin 2\theta e^{i\chi} & -2\sin^2\theta e^{2i\chi} \\ -\frac{2}{\sqrt{2}}\sin 2\theta e^{-i\chi} & 4\cos^2\theta & \frac{2}{\sqrt{2}}\sin 2\theta e^{i\chi} \\ -2\sin^2\theta e^{-2i\chi} & \frac{2}{\sqrt{2}}\sin 2\theta e^{-i\chi} & 2\sin^2\theta \end{pmatrix}. \tag{A8}$$

The upper/lower signs in the nonflip part of (A8) stand for the $(\ell^-\bar{\nu}_\ell)$ case relevant for the decays $\bar{B}^0 \to D^{(*)+}\ell^-\bar{\nu}_\ell$ and $B^- \to D^{(*)0}\ell^-\bar{\nu}_\ell$, and the $(\ell^+\nu_\ell)$ case relevant for the decays $B^+ \to \bar{D}^{(*)0}\ell^+\nu_\ell$ and $B^0 \to \bar{D}^{(*)-}\ell^+\nu_\ell$. The spin-0/spin-1 interference contribution is given by

$$\begin{aligned}(2q^2v)^{-1}&L_{0\lambda_W}(0,1,\theta,\chi) \\ &= (2q^2v)^{-1}L^*_{\lambda_W,0}(1,0,\theta,\chi) \\ &= \delta_\ell\begin{pmatrix} -\frac{4}{\sqrt{2}}\sin\theta e^{-i\chi} & 4\cos\theta & \frac{4}{\sqrt{2}}\sin\theta e^{i\chi}\end{pmatrix},\end{aligned} \tag{A9}$$

$(\lambda_W = 1, 0, -1)$ and

$$(2q^2v)^{-1}L_{00}(0,0,\theta,\chi) = 4\delta_\ell. \tag{A10}$$

For the $\cos\theta$ distribution of the decay $B \to D^*\ell^-\bar{\nu}_\ell$ written down in Eq. (46), one needs the integrated form of Eq. (A6). One obtains

$$\begin{aligned} W'(\theta) &= \int d\cos\theta^* d\chi/2\pi W'(\theta^*,\theta,\chi) \\ &= 2\sum_{J,J',\lambda_W,\lambda_2}(-1)^{J+J'}\delta_{\lambda_2\lambda_W}H_{\lambda_2\lambda_W}(J)H^*_{\lambda_2\lambda_W}(J') \\ &\quad\times L_{\lambda_W\lambda_W}(J,J',\theta), \end{aligned} \tag{A11}$$

where

$$L_{\lambda_W\lambda_W}(J,J',\theta) = \int d\chi/2\pi L_{\lambda_W\lambda_W}(J,J',\theta,\chi). \tag{A12}$$

The integration (A12) is easily done. The result is given by Eqs. (A8) and (A9), where all terms proportional to $e^{\pm i\chi}$, $e^{-\pm 2i\chi}$ have been dropped. The $\cos\theta$ distribution for $B \to D\ell^-\bar{\nu}_\ell$ written down in Eq. (46) is obtained from (A11) by omitting $\delta_{\lambda_2\lambda_W}$ and dropping the label λ_2.

[1] R. Aaij *et al.* (LHCb Collaboration), Measurement of the Ratio of Branching Fractions $\mathcal{B}(\bar{B}^0 \to D^{*+}\tau^-\bar{\nu}_\tau)/\mathcal{B}(\bar{B}^0 \to D^{*+}\mu^-\bar{\nu}_\mu)$, Phys. Rev. Lett. **115**, 111803 (2015); **115**, 159901(E) (2015).

[2] K. Ikado *et al.* (Belle Collaboration), Evidence of the Purely Leptonic Decay $B \to \tau\bar{\nu}_\tau$, Phys. Rev. Lett. **97**, 251802 (2006).

[3] K. Hara *et al.* (Belle Collaboration), Evidence for $B^- \to \tau^-\bar{\nu}_\tau$ with a Hadronic Tagging Method Using the Full Data Sample of Belle, Phys. Rev. Lett. **110**, 131801 (2013).

[4] M. Bona *et al.* (UTfit Collaboration), An improved Standard Model prediction of $BR(B \to \tau\bar{\nu}_\tau)$ and its implications for New Physics, Phys. Lett. B **687**, 61 (2010).

[5] A. Abdesselam *et al.* (Belle Collaboration), Measurement of the branching fraction of $B^+ \to \tau^+\nu_\tau$ decays with the semileptonic tagging method and the full Belle data sample, arXiv:1409.5269.

[6] S. Fajfer, J. F. Kamenik, I. Nisandzic, and J. Zupan, Implications of Lepton Flavor Universality Violations in B-Decays, Phys. Rev. Lett. **109**, 161801 (2012).

[7] P. del Amo Sanchez *et al.* (*BABAR* Collaboration), Study of $B \to \pi\ell\nu$ and $B \to \rho\ell\nu$ decays and determination of $|V_{ub}|$, Phys. Rev. D **83**, 032007 (2011).

[8] H. Ha *et al.* (Belle Collaboration), Measurement of the decay $B^0 \to \pi^-\ell^+\nu$ and determination of $|V_{ub}|$, Phys. Rev. D **83**, 071101 (2011).

[9] D. Asner *et al.* (Heavy Flavor Averaging Group), Averages of b-hadron, c-hadron, and τ-lepton properties, arXiv: 1010.1589.

[10] J. Lees *et al.* (*BABAR* Collaboration), Evidence for an Excess of $\bar{B} \to D^{(*)}\tau^-\bar{\nu}_\tau$ Decays, Phys. Rev. Lett. **109**, 101802 (2012).

[11] M. Huschle *et al.* (Belle Collaboration), Measurement of the branching ratio of $\bar{B} \to D^{(*)}\tau^-\bar{\nu}_\tau$ relative to $\bar{B} \to D^{(*)}\ell^-\bar{\nu}_\ell$ decays with hadronic tagging at Belle, Phys. Rev. D **92**, 072014 (2015).

[12] Z. Ligeti, Flavor Physics and CP Violation 2015, https://agenda.hepl.phys.nagoya-u.ac.jp/indico/getFile.py/access?contribId=9&sessionId=19&resId=0&materialId=slides&confId=170.

[13] M. Tanaka and R. Watanabe, τ-longitudinal polarization in $B \to D\tau\bar{\nu}_\tau$ and its role in the search for charged Higgs boson, Phys. Rev. D **82**, 034027 (2010).

[14] S. Fajfer, J. F. Kamenik, and I. Nisandzic, On the $B \to D^*\tau\bar{\nu}_\tau$ sensitivity to New Physics, Phys. Rev. D **85**, 094025 (2012).

[15] J. F. Kamenik and F. Mescia, $B \to D\tau\bar{\nu}_\tau$ branching ratios: Opportunity for lattice QCD and hadron colliders, Phys. Rev. D **78**, 014003 (2008).

[16] W. S. Hou, Enhanced charged Higgs boson effects in $B \to \tau\bar{\nu}_\tau$, $B \to \mu\bar{\nu}_\mu$ and $b \to \tau\bar{\nu}_\tau + X$, Phys. Rev. D **48**, 2342 (1993).

[17] S. Baek and Y. G. Kim, Constraints on the R-parity violating couplings from $B \to \ell\bar{\nu}_\ell$-decays, Phys. Rev. D **60**, 077701 (1999).

[18] A. Crivellin, J. Heeck, and P. Stoffer, A perturbed lepton-specific two-Higgs-doublet model facing experimental hints for physics beyond the Standard Model, arXiv:1507.07567.

[19] A. Crivellin, C. Greub, and A. Kokulu, Explaining $B \to D\tau\nu$, $B \to D^*\tau\nu$ and $B \to \tau\nu$ in a 2HDM of type III, Phys. Rev. D **86**, 054014 (2012).

[20] S. P. Martin, A supersymmetry primer, Adv. Ser. Dir. High Energy Phys. **21**, 1 (2010).

[21] W. Buchmüller, R. Rückl, and D. Wyler, Leptoquarks in lepton-quark collisions, Phys. Lett. B **191**, 442 (1987).

[22] L. Calibbi, A. Crivellin, and T. Ota, Effective Field Theory Approach to $b \to s\ell\ell^{(\prime)}$, $B \to K^{(*)}\nu\bar{\nu}$ and $B \to D^{(*)}\tau\nu$ with Third Generation Couplings, Phys. Rev. Lett. **115**, 181801 (2015).

[23] A. Datta, M. Duraisamy, and D. Ghosh, Diagnosing New Physics in $b \to c\tau\nu_\tau$ decays in the light of the recent *BABAR* result, Phys. Rev. D **86**, 034027 (2012).

[24] M. Tanaka and R. Watanabe, New physics in the weak interaction of $\bar{B} \to D^{(*)}\tau\bar{\nu}$, Phys. Rev. D **87**, 034028 (2013).

[25] P. Biancofiore, P. Colangelo, and F. De Fazio, On the anomalous enhancement observed in $B \to D^{(*)}\tau\bar{\nu}_\tau$ decays, Phys. Rev. D **87**, 074010 (2013).

[26] M. Neubert, Heavy quark symmetry, Phys. Rep. **245**, 259 (1994).

[27] A. G. Grozin, Heavy Quark Effective Theory, *Springer Tracts in Modern Physics Vol. 201* (Springer-Verlag, Berlin, 2004).

[28] T. Branz, A. Faessler, T. Gutsche, M. A. Ivanov, J. G. Körner, and V. E. Lyubovitskij, Relativistic constituent quark model with infrared confinement, Phys. Rev. D **81**, 034010 (2010).

[29] M. A. Ivanov, J. G. Körner, S. G. Kovalenko, P. Santorelli, and G. G. Saidullaeva, Form factors for semileptonic, non-leptonic and rare $B(B_s)$ meson decays, Phys. Rev. D **85**, 034004 (2012).

[30] D. Ebert, R. N. Faustov, and V. O. Galkin, Relativistic treatment of the decay constants of light and heavy mesons, Phys. Lett. B **635**, 93 (2006).

[31] D. Ebert, R. N. Faustov, and V. O. Galkin, New analysis of semileptonic B decays in the relativistic quark model, Phys. Rev. D **75**, 074008 (2007).

[32] R. N. Faustov and V. O. Galkin, Exclusive weak B decays involving τ lepton in the relativistic quark model, Mod. Phys. Lett. A **27**, 1250183 (2012).

[33] A. Salam, Lagrangian theory of composite particles, Nuovo Cimento **25**, 224 (1962).

[34] S. Weinberg, Elementary particle theory of composite particles, Phys. Rev. **130**, 776 (1963).

[35] G. V. Efimov and M. A. Ivanov, Confinement and quark structure of light hadrons, Int. J. Mod. Phys. A **04**, 2031 (1989).

[36] G. V. Efimov and M. A. Ivanov, *The Quark Confinement Model Of Hadrons*, (Taylor & Francis, London, 1993).

[37] A. Faessler, T. Gutsche, M. A. Ivanov, J. G. Körner, and V. E. Lyubovitskij, Semileptonic decays of double heavy baryons, Phys. Lett. B **518**, 55 (2001).

[38] C. Anastasiou, E. W. N. Glover, and C. Oleari, The two loop scalar and tensor pentabox graph with lightlike legs, Nucl. Phys. **B575**, 416 (2000); **B585**, 763(E) (2000).

[39] M. R. Fiorentin, FaRe: A Mathematica package for tensor reduction of Feynman integrals, Int. J. Mod. Phys. C **27**, 1650027 (2015).

[40] T. Gutsche, M. A. Ivanov, J. G. Körner, V. E. Lyubovitskij, P. Santorelli, and N. Habyl, Semileptonic decay $\Lambda_b \to \Lambda_c + \tau^- + \bar{\nu}_\tau$ in the covariant confined quark model, Phys. Rev. D **91**, 074001 (2015); **91**, 119907(E) (2015).

[41] G. Ganbold, T. Gutsche, M. A. Ivanov, and V. E. Lyubovitskij, On the meson mass spectrum in the covariant confined quark model, J. Phys. G **42**, 075002 (2015).

[42] A. Issadykov, M. A. Ivanov, and S. K. Sakhiyev, Form factors of the B–S-transitions in the covariant quark model, Phys. Rev. D **91**, 074007 (2015).

[43] S. S. Gershtein and M. Y. Khlopov, Lepton decays of heavy pseudoscalar meson, Pis'ma Zh. Eksp. Teor. Fiz. **23**, 374 (1976) [JETP Lett. **23**, 338 (1976)].

[44] M. Y. Khlopov, Effects of symmetry violation in semi-leptonic meson decays, Yad. Fiz. **28**, 1134 (1978) [Sov. J. Nucl. Phys. **28**, 583 (1978)].

[45] K. A. Olive *et al.* (Particle Data Group), Review of particle physics, Chin. Phys. C **38**, 090001 (2014).

[46] A. Bazavov *et al.* (Fermilab Lattice Collaboration, MILC Collaboration), B- and D-meson decay constants from three-flavor lattice QCD, Phys. Rev. D **85**, 114506 (2012).

[47] A. Gray, M. Wingate, C. T. H. Davies, E. Gulez, G. P. Lepage, Q. Mason, M. Nobes, and J. Shigemitsu (HPQCD Collaboration), The B Meson Decay Constant from Unquenched Lattice QCD, Phys. Rev. Lett. **95**, 212001 (2005).

[48] M. D. Morte, S. Durr, D. Guazzini, R. Sommer, J. Heitger *et al.*, Heavy-strange meson decay constants in the continuum limit of quenched QCD, J. High Energy Phys. 02 (2008) 078.

[49] T. W. Chiu, T. H. Hsieh, C. H. Huang, and K. Ogawa (TWQCD Collaboration), Beauty mesons in lattice QCD with exact chiral symmetry, Phys. Lett. B **651**, 171 (2007).

[50] D. Becirevic, Ph. Boucaud, J. P. Leroy, V. Lubicz, G. Martinelli, F. Mescia, and F. Rapuano, Nonperturbatively improved heavy-light mesons: Masses and decay constants, Phys. Rev. D **60**, 074501 (1999).

[51] W. Lucha, D. Melikhov, and S. Simula, Decay constants of beauty mesons from QCD sum rules, EPJ Web Conf. **80**, 00046 (2014).

[52] D. Becirevic, V. Lubicz, F. Sanfilippo, S. Simula, and C. Tarantino, D-meson decay constants and a check of

factorization in non-leptonic B-decays, J. High Energy Phys. 02 (2012) 042.
[53] W. Lucha, D. Melikhov, and S. Simula, Decay constants of the charmed vector mesons D^* and D_s^* from QCD sum rules, Phys. Lett. B **735**, 12 (2014).
[54] D. Becirevic, N. Kosnik, and A. Tayduganov, $\bar{B} \to D\tau\bar{\nu}_\tau$ VS $\bar{B} \to D\mu\bar{\nu}_\mu$Phys. Lett. B **716**, 208 (2012).
[55] M. A. Ivanov, O. E. Khomutenko, and T. Mizutani, Form-factors of semileptonic decays of heavy mesons in the quark confinement model, Phys. Rev. D **46**, 3817 (1992).
[56] M. A. Ivanov, Y. L. Kalinovsky, and C. D. Roberts, Survey of heavy meson observables, Phys. Rev. D **60**, 034018 (1999).
[57] A. Faessler, T. Gutsche, M. A. Ivanov, J. G. Körner, and V. E. Lyubovitskij, The exclusive rare decays $B \to \mathrm{K}(\mathrm{K}*)\bar{\ell}\ell$ and $B_c \to \mathrm{D}(\mathrm{D}*)\bar{\ell}\ell$ in a relativistic quark model, Eur. Phys. J. direct C **4**, 18 (2002).
[58] We take this opportunity to correct a typo in Ref. [40]. The factor $-3/2$ in Eq. (38) of Ref. [40] should read $-3/4$.
[59] J. G. Körner and G. A. Schuler, Exclusive semileptonic decays of bottom mesons in the spectator quark model, Z. Phys. C **38**, 511 (1988); **41**, 690(E) (1989).
[60] J. G. Körner and G. A. Schuler, Exclusive semileptonic heavy meson decays including lepton mass effects, Z. Phys. C **46**, 93 (1990).
[61] J. G. Körner and G. A. Schuler, Lepton mass effects in semileptonic B-meson decays, Phys. Lett. B **231**, 306 (1989).
[62] K. Hagiwara, A. D. Martin, and M. F. Wade, Exclusive semileptonic B-meson decays, Nucl. Phys. **B327**, 569 (1989).
[63] J. Charles, A. Höcker, H. Lacker, S. Laplace, F. R. Diberder, J. Malclés, J. Ocariz, M. Pivk, and L. Roos (CKMfitter Group), CP violation and the CKM matrix: Assessing the impact of the asymmetric B factories, Eur. Phys. J. C **41**, 1 (2005).
[64] B. Aubert *et al.* (*BABAR* Collaboration), A Measurement of the Branching Fractions of Exclusive $\bar{B} \to D^{(*)}(\pi)\ell^-\bar{\nu}_\ell$ Decays in Events with a Fully Reconstructed B Meson, Phys. Rev. Lett. **100**, 151802 (2008).
[65] S. Berge, S. Groote, J. G. Körner, and L. Kaldamäe, Lepton-mass effects in the decays $H \to ZZ^* \to \ell^+\ell^-\tau^+\tau^-$ and $H \to WW^* \to \ell\nu\tau\nu_\tau$, Phys. Rev. D **92**, 033001 (2015).
[66] The choice of the unitary gauge is dictated by electroweak gauge invariance.